

Density Functionals for Hydrogen Storage: Defining the H2Bind275 Test Set with Ab Initio Benchmarks and Assessment of 55 Functionals

Srimukh Prasad Veccham* and Martin Head-Gordon*

Department of Chemistry, University of California, Berkeley, California 94720, USA
Chemical Sciences Division, Lawrence Berkeley National Laboratory, Berkeley, California
94720, USA

E-mail: srinukh.prasad@berkeley.edu; [mhc@cchem.berkeley.edu](mailto:mhg@cchem.berkeley.edu)

Abstract

Efficient and high capacity storage materials are indispensable for a hydrogen-based economy. In silico tools can accelerate the process of discovery of new adsorbent materials with optimal hydrogen adsorption enthalpies. Density functional theory is well-poised to become a very useful tool for enabling high-throughput screening of potential materials. In this work, we have identified density functional approximations that provide good performance for hydrogen binding applications following a two-pronged approach. First, we have compiled a dataset (H2Bind275) that comprehensively represents the hydrogen binding problem capturing the chemical and mechanistic diversity in the binding sites encountered in hydrogen storage materials. We have also computed reference interaction energies for this dataset using coupled cluster theory. Secondly, we have assessed the performance of 55 density functional approximations for predicting H₂ interaction energies and have identified two hybrid density functionals (ω B97X-V and ω B97M-V), two double hybrid density functionals (DSD-PBEPBE-D3(BJ) and PBE0-DH), and one semi-local density functional (B97M-V) as the best performing ones. We have recommended the addition of empirical dispersion corrections to systematically underbinding density functionals like revPBE, BLYP, and B3LYP for improvements in performance at negligible additional cost. We have also recommended the usage of the def2-TZVPP basis set as it represents a good compromise between accuracy and cost, limiting the finite basis set errors to less than 1kJ/mol.

Introduction

Hydrogen (H_2) is a promising green alternative to the fossil fuel-based energy economy. H_2 is a clean fuel as the only byproduct it produces is water, which is non-toxic and unlike CO_2 has no deleterious effects on the environment. The gravimetric energy capacity of hydrogen is also about three times that of gasoline, providing a mass-efficient way to store and transport energy. One major problem with using H_2 as fuel is the low volumetric capacity of hydrogen which is one of the biggest hurdles in achieving a H_2 -based economy.

One solution to this volumetric capacity obstacle is to store hydrogen in tanks under high pressure. Hydrogen fuel cell vehicles with high pressure carbon fiber-reinforced tanks are already on the market. However, safely storing H_2 under high pressure adds a substantial cost penalty, not to mention the additional safety complications associated with accidents. Nanoporous materials with high surface area offer a viable alternative to this storage problem by storing H_2 in adsorbed form. In principle, a given quantity of H_2 can be stored by adsorption at a much lower pressure in comparison to pure compression. Despite major synthetic and design efforts in the nanoporous framework community, none of the materials designed till date have been able to achieve all the targets for a viable storage material compiled by the U.S. Department of Energy (DOE).¹ While some recently synthesized materials have come close to the target,² novel design strategies and new material discoveries are still required to achieve the DOE targets.

Nanoporous sorbent materials, including Metal-Organic Frameworks (MOFs) and Covalent Organic Frameworks (COFs), represent the vast majority of storage materials proposed to date for hydrogen. For example, H_2 storage by binding to open metal sites with unsaturated coordination spheres in MOFs has successfully been explored in MOF-11,³ $M_2(\text{dobdc})$,⁴ and Mn-BTT.⁵ Covalent Organic Frameworks which are robust both structurally and thermally, represent another paradigm for H_2 storage.⁶ Enhancement of hydrogen storage capacities by impregnation with metal ions is an active area of research. Graphene, graphene oxide, and graphene origami are new carbon-based adsorbents that have been explored for

hydrogen storage.⁷⁻⁹ Given this huge diversity in the binding moieties of H₂, we feel it is necessary to have a dataset that captures this variety appropriately. The dataset compiled in this work aims to capture the diversity only in materials that store H₂ by adsorption, and not other materials which store H₂ by hydrogenation/dehydrogenation of molecules.^{10?}

In silico tools have become indispensable in the design of drugs, proteins, and materials with desired properties using both rational and high-throughput design strategies. In the context of designing materials for hydrogen storage, researchers are seeking frameworks with the highest usable capacity for a predetermined operating pressure range. The usable capacity is the difference between the amount of hydrogen adsorbed at high and low operating pressures. The usable capacity is completely determined by the adsorption isotherm of H₂, which in turn is influenced by the Gibbs free energy of adsorption, pore volume and surface area in the region where Henry’s law is applicable. The Gibbs free energy of adsorption ΔG_{ads} , in turn, can be determined by the enthalpy (ΔH_{ads}) and entropy (ΔS_{ads}) of adsorption at a given temperature (T) according to Eq. (1)

$$\Delta G_{ads} = \Delta H_{ads} - T\Delta S_{ads} \tag{1}$$

Enthalpy and entropy are known to be roughly correlated, even though the exact relationship depends on the adsorbent material.¹¹⁻¹³ The most important component of enthalpy is the internal energy of binding at 0K which can be predicted with very good accuracy using different first principles tools of electronic structure theory. Common first principles tools that can be used to predict binding energy are Hartree Fock (HF), Density Functional Theory (DFT), second order Møller-Plesset Perturbation Theory (MP2), Configuration Interaction (CI), and different variants of Coupled Cluster theory (CC). These methods can predict binding energies with different degrees of accuracy. The associated computational cost is also very different with HF and DFT scaling as $\mathcal{O}(N^3)$, MP2 as $\mathcal{O}(N^5)$, and Coupled Cluster with Singles, Doubles and Perturbative Triples (CCSD(T)) as $\mathcal{O}(N^7)$. Of these methods,

CCSD(T) provides the highest accuracy: typically yielding sub-kJ/mol accuracy for non-covalent interaction energies.¹⁴ However, the need for thousands of calculations in a high-throughput screening along with its steep scaling in computational cost makes it impossible to use coupled cluster theory for designing materials.

DFT, with $\mathcal{O}(N^3)$ scaling, lies at a reasonable compromise between accuracy and cost for predicting binding energies. While in principle, DFT can provide an exact solution to the Schrodinger equation under the Born-Oppenheimer approximation, the exact form of this functional remains unknown.¹⁵ Over the last couple of decades, various groups across the world have proposed different approximations to this functional form using empirical, semi-empirical, and non-empirical arguments. There are hundreds of these approximations, termed density functional approximations (DFAs), and each of them provides different accuracies for different problems including non-covalent interactions, reaction barrier heights, thermochemistry, and ionization energies. Some density functionals have also been parameterized to predict properties of certain classes of chemical species limiting their applicability to other classes. In fact, different DFAs have previously been used to predict the deliverable capacity for various storage materials.¹⁶⁻²¹ Even though the performance of DFAs have been thoroughly benchmarked²²⁻²⁵ for each of these properties (represented by one or multiple datasets), none of them thoroughly represents the hydrogen storage problem. In fact, to the best of our knowledge, none of the datasets even contain the hydrogen molecule. In this paper, we have compiled a dataset that captures the diversity of binding sites encountered in materials that adsorb hydrogen.

Another computational approach to determine the usable capacity of a material is using Grand Canonical Monte Carlo (GCMC) simulations which rely on force fields to accurately reproduce the interactions between the adsorbate (H_2) and the binding motifs. As these simulations need a large number of energy evaluations, they are usually performed using force fields. It is also possible to perform simulations directly using DFT at the expense of greater computational cost.²⁶ Parameterization of force fields require highly accurate ab

initio data which can be generated, in principle, using density functional approximations.

Cluster modeling, that is reducing the size of the binding site to a few atoms at the immediate vicinity of the bound H_2 employing suitable chemical truncation, is often used to make extended adsorbent materials with well-defined binding sites computationally tractable.^{17,27,28} The alternative to cluster modeling is to use periodic boundary conditions which would severely limit the usage of highly accurate wavefunction methods. In this work, we have employed cluster models in order to obtain reference interaction energies with high accuracy. Small cluster models also allow for modeling of the binding site instead of a particular binding material, thereby increasing the transferability of the conclusions to other binding materials with similar binding sites.

This paper is organized as follows: The H2Bind275 dataset is introduced and its ability to comprehensively represent the diversity of H_2 binding sites and mechanisms is discussed. The protocol used for arriving at accurate reference interaction energies using coupled cluster theory with the focal point analysis is introduced. After a brief discussion of the performance of wavefunction methods, the performance of 55 density functionals is assessed and the best performing density functional approximations are identified. This assessment is performed for the whole H2Bind275 dataset and different chemical categories of the dataset, motivated by H_2 storage applications. The effect of addition of exact exchange and empirical dispersion corrections to DFAs is analyzed. The problems associated with using finite-sized basis sets for DFT calculations are discussed.

Computational details

All the density functional approximation interaction energies were computed using Q-Chem 5.0.²⁹ The reference interaction energies including MP2, CCSD, and CCSD(T) were also computed using Q-Chem 5.0. Post CCSD(T) computations, specifically CCSDT(Q), were performed using the MRCC program which is capable of performing arbitrary order coupled-

cluster theory.³⁰⁻³² In order to ensure consistency across different quantum chemistry programs, we compared and verified HF and MP2 energies across both the programs. The CCSDT(Q) calculations were performed using 6-31G**(mod), a modified 6-31G** basis set where 0.35, 0.25, and 0.15 are the exponents of the f-type, d-type, and p-type polarization functions respectively. This basis set was found to give outstanding results for non-covalent interaction energies in the A24 dataset despite its small size.^{33,34}

Mechanism of H₂ binding

The factors involved in H₂ interaction with binding motifs can be broadly classified into two categories: (1) physisorption (2) chemisorption. Physisorption includes the electrostatic and induced electrostatic interactions of H₂. H₂ is an uncharged molecule with a permanent quadrupole moment. As a consequence, permanent electrostatics are expected to be very weak. However, a dipole can be induced in the presence of a strong electric field and H₂ can interact with the binding site through polarization. However, H₂'s large HOMO-LUMO gap of 11.19 eV makes this interaction difficult and significant polarization only occurs in the presence of very strong electric fields, like those created by unscreened charges of open metal sites.²⁸ Another significant mechanism of interaction is charge transfer which occurs as a part of chemisorption. Charge transfer from the σ_g -bond orbital of H₂ to the binding site is the most common form of interaction as it can occur with any binding site. H₂ can also participate in a Kubas-like synergistic interaction wherein it interacts with transition metals through both forward ($\sigma_g(\text{H}_2) \rightarrow d(\text{M})$) and backward donation ($d(\text{M}) \rightarrow \sigma_u^*(\text{H}_2)$).³⁵⁻³⁷ While these Kubas-like interactions are too strong for H₂ storage applications, interaction tuning by changing the ligand framework around the transition metal can still make this mechanism important for storage applications.

H2Bind275 Dataset

As none of the existing non-covalent interaction energy datasets represent the H₂ binding problem comprehensively, we have compiled a new dataset which adequately represents the diversity in the H₂ binding motifs and mechanisms of interaction. Each geometry in the dataset, here after referred to as H2Bind275, consists of representative binding motifs interacting with one or multiple H₂ molecules. Development of materials with multiple H₂ binding at a single site is a promising strategy for making materials with enhanced uptake.^{38,39} The H2Bind275 dataset has many data points with multiple H₂s binding to a single site, and is consistent with this encouraging paradigm. Each geometry has been optimized using the density functional ω B97M-V⁴⁰ in the def2-TZVPD basis set⁴¹ in order to ensure maximum interaction with the binding the motif. The optimized geometry has been confirmed to be a minimum on the potential energy surface by ensuring that the hessian has no negative eigenvalues. All the geometries chosen are also in their ground spin state at equilibrium. We have also assessed that using ω B97M-V geometries does not induce any bias in the dataset (See Table S4 and associated discussion for further information). The dataset can be broadly classified into four categories: (1) s-block ions (2) salts (3) organic ligands (4) transition metals.

s-block ions: This category consists of alkali and alkaline earth metal ions with an unscreened charge binding one or multiple H₂ molecules. Post synthetic modification is a common strategy to incorporate H₂ binding entities in porous materials like MOFs. Open metal sites consisting of s-block metal ions have been proposed as promising candidates for exhibiting an enhanced uptake of H₂.^{17,42} With regard to this, we have included Li⁺, Na⁺, Mg²⁺, and Ca²⁺ with one or multiple hydrogens bound as a representative sample of s-block ions constituting open metal sites. This category consists of 19 unique geometries with 77 different interaction energies.

Salts: This category consists of small inorganic salts like AlF₃, CaCl₂, CaF₂, and MgF₂ binding one or multiple H₂ molecules. While it would be highly desirable to incorporate

open metal sites with unscreened charge in porous materials, it is generally hard because of their high reactivity. Metals ions are thus found in their screened forms, and these four inorganic salts form a good representation of such binding motifs.

Organic ligands: Porous materials like MOFs and Covalent Organic Frameworks consist of organic linker molecules connecting metal ions or clusters. While linkers might not be the main binding sites contributing to H₂ uptake, they represent a large surface area that the H₂ interacts with. This set consists of both aromatic and aliphatic organic ligands interacting with one H₂ molecule.

Transition metals: Many MOFs binding H₂ consist of transition metals or transition metal clusters at secondary binding units or open metal sites. This subset consists of mono-cationic 3d transition metals binding 1–4 H₂ molecules. For instance, Cr⁺ bound to 1–4 H₂ belongs to this subset. Most of these species have been experimentally isolated and characterized and have also been theoretically well-studied.⁴³ In order to include species with screened charge, we have included species like hydrides, fluorides, and chlorides of copper, silver and gold, a few of which have been experimentally and theoretically studied earlier.^{44–46} We have also included certain other species like CoF₃, CrCl₂, CuCN, Ni(OH)₂ in order to capture the diversity in the transition metal binding sites.

In summary, as shown in Table. 1 and Fig. (1), the H2Bind275 dataset, consisting of 86 unique geometries and 275 interaction energies, represents the problem of hydrogen binding in porous frameworks reasonably comprehensively.

Table 1: A table showing the number of unique geometries and interaction energies in each category of the dataset

	s-block ions	Salts	Organic ligands	Transition metals	Total
Geometries	19	13	5	49	86
Data points	77	44	10	144	275

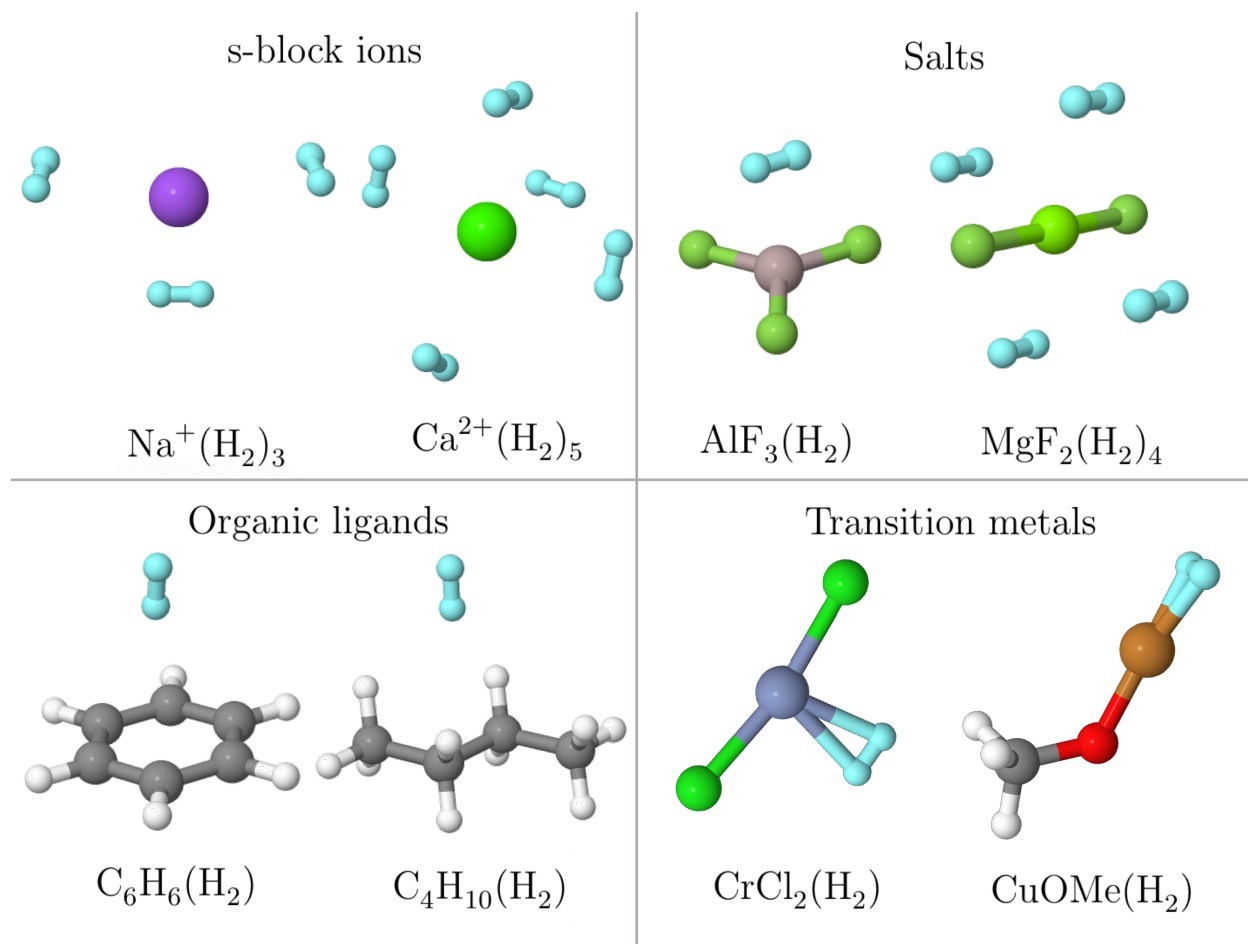


Figure 1: A figure showing instances of the H2Bind275 dataset categorized as s-block ions, salts, organic ligands, and transition metals.

Reference interaction energies

Coupled cluster theory was used to compute the reference interaction energies for this dataset. Coupled cluster with singles, doubles, and perturbative triples (CCSD(T))⁴⁷ is well-known to give high accuracy for non-covalent interactions and has been dubbed the “gold standard” of quantum chemistry.¹⁴ Defining N as the number of basis functions, the steep $\mathcal{O}(N^7)(N^7)$ asymptotic scaling of computational cost of CCSD(T) together with the slow convergence of correlation energies with size of the basis set presents a huge hurdle to using CCSD(T) with large basis sets even for small molecules. In order to circumvent this problem, composite extrapolation procedures like the Gaussian- n models,^{48–51} Weizmann- n models,^{52–54} HEAT,⁵⁵ and ccCA⁵⁶ have been routinely employed. These procedures leverage the varying convergence rates of different components of interaction energy and additivity of different correlation energies to calculate molecular properties with sub-kJ/mol accuracy.

In this work, we use the composite CCSD(T) method as shown in (2).

$$E_{\text{ref}} = E_{\text{HF}/5Z} + E_{\text{MP2}/\text{QZ} \rightarrow 5Z} + \delta E_{\text{CCSD(T)}/\text{TZ}} + \delta E_{\text{MP2}/\text{TZ}}^{\text{core}} \quad (2)$$

$$\delta E_{\text{CCSD(T)}/\text{TZ}} = E_{\text{CCSD(T)}/\text{TZ}} - E_{\text{MP2}/\text{TZ}} \quad (3)$$

$$\delta E_{\text{MP2}/\text{TZ}}^{\text{core}} = E_{\text{MP2}/\text{TZ}}^{\text{core}=0} - E_{\text{MP2}/\text{TZ}}^{\text{core}=n} \quad (4)$$

In the composite scheme, the interaction energy is divided into the mean-field and correlation components. The mean-field component is computed using Hartree Fock (HF) theory with a basis set of quintuple-zeta quality and is labelled as $E_{\text{HF}/5Z}$. The correlation part is computed using the focal point analysis^{57,58} which is at the heart of many of the composite methods mentioned previously. The MP2 correlation energy is extrapolated to the basis set limit using quadruple-zeta and quintuple-zeta quality basis sets with the HKKN extrapolation formula⁵⁹ and is denoted as $E_{\text{MP2}/\text{QZ} \rightarrow 5Z}$. The CCSD(T) correction to the MP2 correlation energy (labelled $\delta E_{\text{CCSD(T)}/\text{TZ}}$), defined as the difference between the CCSD(T) ($E_{\text{CCSD(T)}/\text{TZ}}$) and MP2 ($E_{\text{MP2}/\text{TZ}}$) correlation energies, was added at a triple-zeta quality basis. The effect

of the core-valence electron correlation was computed using MP2 at a triple-zeta quality basis set and is denoted as $\delta E_{\text{MP2/TZ}}^{\text{core}}$. This effect is computed as the difference in the MP2 correlation energies with and without freezing core electrons (denoted as $E_{\text{MP2/TZ}}^{\text{core}=\text{n}}$ and $E_{\text{MP2/TZ}}^{\text{core}=0}$ respectively). Correlation consistent Dunning basis sets were employed to compute each of the components of the reference interaction energy. The cc-pVnZ^{60,61} family of basis sets were used when all core electrons were frozen in correlation calculations and the cc-pCVnZ^{62,63} family was used when only a part or none of the core was frozen. For transition metals, the cc-pwCVnZ⁶⁴ family was used with a neon frozen core. The effect of freezing core-valence correlations is discussed later in this section.

In this section, we attempt to isolate and characterize the different sources of error arising from using this protocol and subsequently justify the parameters used in this protocol. In the benchmark protocol fixed in Eq. (2), there can be three major sources of errors: (1) errors arising from using a finite basis set, (2) errors from neglecting higher order terms in coupled cluster theory, and (3) errors from using the frozen core approximation for correlated calculations.

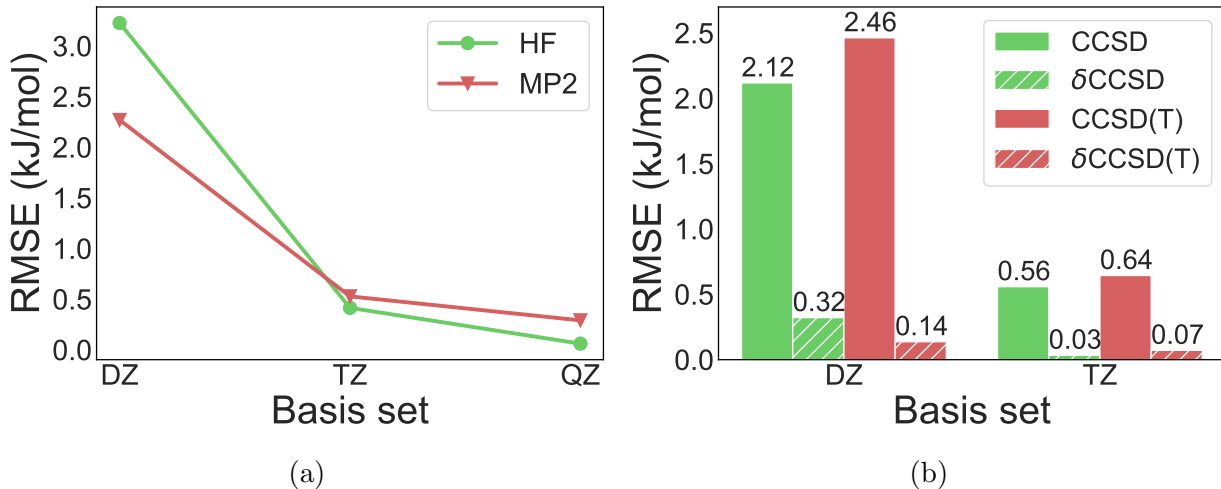


Figure 2: (a) Basis set convergence properties of HF energy and MP2 correlation energies at double-zeta (DZ), triple-zeta(TZ), and quadruple-zeta (QZ) quality basis sets. Errors are with respect to quintuple-zeta basis sets (5Z) (b) Basis set convergence properties of CCSD and CCSD(T) terms contrasted with the convergence properties of δ CCSD and δ CCSD(T) terms at double-zeta (DZ) and triple-zeta (TZ) quality basis sets. The errors are with respect to the quadruple-zeta (QZ) quality basis sets.

In order to ensure that each of the terms in Eq. (2) is converged with respect to the size of the basis set, we investigated the convergence properties of each of these terms over a small subset of the H2Bind275 dataset as shown in Fig. (2). The SCF interaction energy converges roughly exponentially with the cardinality of the basis set which can be seen from Fig. (2)(a).⁶⁵ The RMSD between the HF interaction energies at quadruple-zeta and quintuple-zeta basis sets is only 0.06 kJ/mol and hence we have used the HF at quintuple-zeta quality basis set without any further extrapolation. The MP2 correlation energy, however, converges only polynomially with cardinal number, leading to a substantially larger difference of 0.29 kJ/mol between quadruple-zeta and quintuple-zeta basis sets. The HKKN formula used to extrapolate the MP2 correlation energy recovers an additional RMS interaction correlation energy of 0.30 kJ/mol that is not captured at the 5Z basis level. The convergence of the CCSD and CCSD(T) correlation energies are also slow with respect to the size of the basis set as shown in Fig. (2)(b). The deviation in the CCSD(T) interaction correlation energies at triple-zeta quality basis set is 0.64 kJ/mol (RMSD) from those at the quadruple-zeta quality basis set. The focal point analysis method used in Eq. (2) circumvents this problem by computing only the difference in correlation energy between CCSD(T) and MP2 ($\delta E_{\text{CCSD(T)}}$ term). This difference term converges much more quickly with respect to the size of the basis set with a difference of only 0.07 kJ/mol between the triple-zeta and quadruple-zeta quality basis sets. Of the binding motifs investigated in this study, the Mg^{2+} species binding one or multiple hydrogens will exert the strongest electric field on hydrogen(s) because of its large charge density. This strong electric field would distort and shift the density on H_2 more than other binding motifs. Diffuse basis functions are required to capture this shift in the density, and Mg^{2+} ion binding motifs should show the maximum deviation in the interaction energies between basis sets containing diffuse functions (aug-cc-pCVnZ) and those that do not (cc-pCVnZ). For the four Mg^{2+} species considered, the RMSD in the interaction energies is only 0.10 kJ/mol with a maximum percent deviation of 0.015%. This represents a soft upper bound to the expected deviation in the interaction energies if the cc-pCVnZ basis sets are

replaced with their augmented counterparts. Given that this deviation is almost negligible and the heightened computational cost involved in using aug-cc-pCVnZ type basis sets, we have used cc-pCVnZ type basis sets for all the reference calculations in this work.

The effect of higher order excitations that were neglected in CCSD(T) was analyzed using CCSDT(Q) in the 6-31G**(mod) basis set which has been shown to yield accurate results for computing the $\delta E_{\text{CCSDT(Q)}}$ terms computed as shown in Eq. (5).

$$\delta E_{\text{CCSDT(Q)}/6-31\text{G}^{**}(\text{mod})} = E_{\text{CCSDT(Q)}/6-31\text{G}^{**}(\text{mod})} - E_{\text{CCSD(T)}/6-31\text{G}^{**}(\text{mod})} \quad (5)$$

For the 118 species whose HF solution matches up between MRCC and Q-Chem, the maximum $\delta E_{\text{CCSDT(Q)}}$ correction was found to be -1.8 kJ/mol with an average correction of 0.2 kJ/mol. The maximum $\delta E_{\text{CCSDT(Q)}}$ correction is seen for the Cu^+ species bound to H_2 whose reference interaction energy is 66.9 kJ/mol. The correction of 1.8 kJ/mol is only 2.8% of the total interaction energy. CCSD(T) shows systematic underbinding for all cases except a few ones like Cu salts and Zn^+ which show a positive value of $\delta E_{\text{CCSDT(Q)}}$. As shown in Fig. S1 of the supplementary information, we can see that most of the $\delta E_{\text{CCSDT(Q)}}$ corrections are nearly zero, justifying the neglect of their contribution in fixing the final reference interaction energies. The $\delta E_{\text{CCSDT(Q)}}$ corrections to the 118 species is provided in the supplementary information.

Core-valence correlations contribute a non-negligible amount to the interaction energy. Just considering the salts subset, the core-valence correlations contribute 3.0 kJ/mol to the reference interaction energy. This quite large contribution of the core-valence correlation energy to the interaction energy was very surprising. In order to account for this effect, the size of the frozen core was made as small as computationally feasible. For the s-block ions and salts subsets, no core electrons were frozen, making the term $\delta E_{\text{MP2/TZ}}^{\text{core}}$ zero. For the organic subset, the effect of core-valence correlations was found to be very small (0.04 kJ/mol) and was therefore taken care of in an additive manner as in equation Eq. (4) using

MP2 and a triple-zeta quality basis set. For the transition metals subset, a neon core was frozen and the effect of freezing it was estimated using MP2 at a triple-zeta quality basis set.

All the calculations were done on the ground electronic and spin state of the species. The s-block ions, salts, and organic categories consist only of closed-shell singlet species with unambiguous ground spin states. For the transition metal category, ground spin state was determined using CCSD(T)/TZ. In cases where experimental references were found, the CCSD(T)/TZ ground spin state agreed with experiments. A table showing the spin state chosen and their experimental references can be found in Table S2. Transition metal containing systems are often tricky to handle as they might exhibit multireference character. Spin-symmetry breaking at the Hartree-Fock level is often required for describing systems with multireference character and hence the existence of spin-symmetry breaking can be used as a diagnostic tool for it.^{66,67} Of the binding motifs chosen, the maximum deviation of $\langle S^2 \rangle$ deviation of 0.018 is exhibited by $\text{Co}^+(\text{H}_2)_4$. This deviation is negligible and hence these orbitals can reliably be used for correlation calculations.

DFT interaction energies were computed using a quadruple-zeta quality Karlsruhe basis, def2-QZVPPD⁴¹ and a quadrature grid consisting of 99 Euler-MacLaurin radial points and 590 Lebedev angular points. SG-1 was used for integrating the non-local VV10 part in functionals that employ it.⁶⁸ There are two additional degrees of freedom for double hybrid density functionals: (1) employment of the density fitting approximation, (2) frozen core approximation. We have used these density functionals as they were trained originally. In cases where the authors did not specify how they were trained, we have used the parameters that give the least error and these details have been documented in Table S1. The reference and density functional interaction energies were computed as the difference between the complex, the substrate, and H_2 , as shown in Eq. (6)

$$\Delta E_{int} = E(\text{M}-(\text{H}_2)_n) - E(\text{M}-(\text{H}_2)_{n-1}) - E(\text{H}_2) \quad (6)$$

where ΔE_{int} is the interaction energy binding one of the H_2 s to the substrate, $E(M-(H_2)_n)$ is the energy of the substrate bound to one or multiple H_2 s, $E(M-(H_2)_{n-1})$ is the energy of the substrate bound to $(n - 1)$ H_2 s at the $M-(H_2)_n$ geometry, and $E(H_2)$ is the energy of the H_2 at the $M-(H_2)_n$ geometry. This is commonly referred to as the “vertical” interaction energy as the geometries of the subsystems are not allowed to relax. Another way to compute energy is to account for the geometric distortion of the substrate and H_2 upon complex formation. In this method, the relaxed geometry for the substrate and H_2 are used in (6). This method of computing interaction energy is called “adiabatic” interaction energy. In this work, we compute the interaction energy for each binding moiety using both the adiabatic and vertical methods.

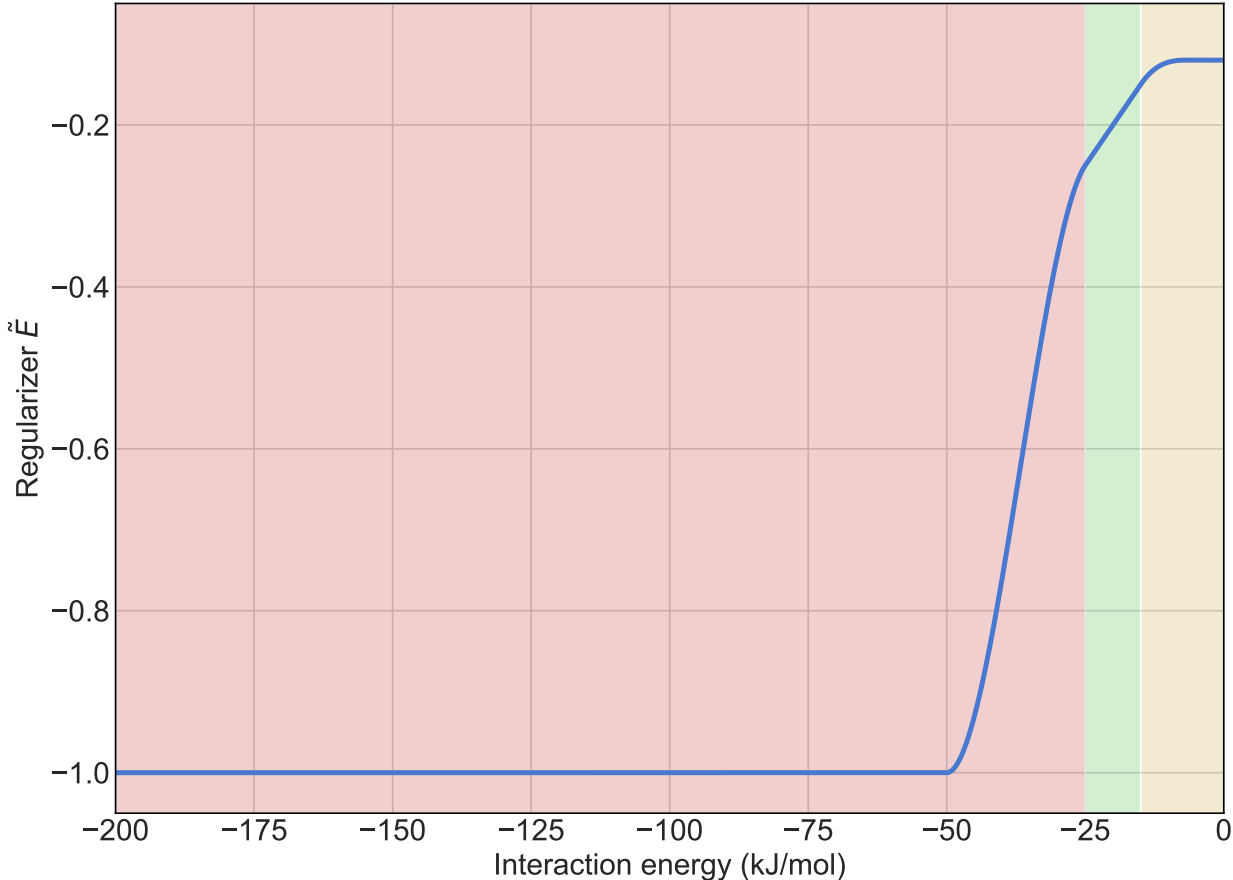


Figure 3: A figure showing the regularizer in the interaction energy regime of -200 to 0 kJ/mol.

The reference binding energies for the H2Bind275 dataset are spread over two orders of

Table 2: A table showing the different error metrics used in the various interaction energy regimes specifically catered to the H₂ binding problem. The error, ΔE , is defined as $\Delta E = |E - \hat{E}|/\tilde{E}$, where \hat{E} is the reference interaction energy and \tilde{E} is the regularizer.

	Energy range	Error metric	Error Formula	Regularizer \tilde{E}
Strong	-200 to -25	Absolute error	$\Delta E = E - \hat{E} $	-1
Favorable	-25 to -15	Relative error	$\Delta E = (\frac{E-\hat{E}}{\hat{E}}) \times 100 $	$\frac{\hat{E}}{100}$
Weak	-15 to 0	Regularized Relative error	$\Delta E = (\frac{E-\hat{E}}{-12}) \times 100 $	$\frac{-12}{100}$

magnitude (*vide infra*). While all the species in the dataset inform us about the performance of density functionals for H₂ binding, not all of them give us the same amount of information. In H₂ storage applications, it is desired to have binding sites with an interaction energy of -15 kJ/mol to -25 kJ/mol for maximum uptake when operated between the pressures of 5 and 100 bar.^{11,69,70} We have designed our error metric so as to give more weight to species in the interaction energy regime of -25 to -15 kJ/mol. The total interaction energy regime, and consequently the binding moieties, were divided into three categories: (1) strong, (2) favorable, and (c) weak. The energy ranges and error metrics used are summarized in Table. (2). The strong category consists of species with binding energies stronger than -25 kJ/mol. The DFT errors in this regime should have smaller weights and hence absolute error was used in this region making the actual magnitude of the errors small. This would imply a regularizer of $\tilde{E} = -1$ in this regime. The favorable regime consists of species with an interaction energy between -25 kJ/mol and -15 kJ/mol. Large weights should be associated with errors in this region as they are of most importance from the H₂ storage perspective. Absolute percentage error is used in this region making the absolute magnitude of the errors relatively large. A regularizer of $\tilde{E} = \hat{E}/100$ was used for this range. Errors in the > -15 kJ/mol region are also important as these represent secondary H₂ binding sites like H₂ binding to organic linker molecules in MOFs. While these sites were not specifically designed to bind H₂, they serve as important structural units that keep the binding sites together. It is important to accurately model these interactions as they also contribute to the overall uptake of the material. However, small values of reference interaction energy

in the denominator could cause the error to blow up and get numerically large weights. This was avoided by using a constant regularized reference of -12 kJ/mol, which implies $\tilde{E} = -12/100$. The comprehensive error metric, Regularized Mean Absolute Percentage Error (RegMAPE), smoothly interpolates between absolute error and percentage error while transitioning from strong to favorable regime and again smoothly interpolates between the percentage error and regularized percentage error while moving from the favorable to weak regime. The regularizer, \tilde{E} , is plotted in Fig. (3).

Results and Discussion

Reference Interaction Energies

The computed reference interaction energies range from -189.0 kJ/mol to -2.3 kJ/mol spanning more than two orders of magnitude. The distribution of the interaction energies can be seen in Fig. (4) which shows the distribution of the reference interaction energies by chemical categories of the dataset. s-block ions, consisting of 77 data points are concentrated in the -10 to -50 kJ/mol region. In contrast, the salts category has a much smaller range of -11 kJ/mol to -25 kJ/mol with 18 data points in the favorable regime. Furthermore, the organic category has an even smaller range with all the species lying between -2.3 kJ/mol and -5.6 kJ/mol. Transition metals, by far, show the most diversity in the interaction energies with values ranging from -5.3 kJ/mol to -189.0 kJ/mol. However, majority of the transition metal containing species have interaction energies of less than 100 kJ/mol. Of the total 275 data points, 50 of them lie in the favorable range for hydrogen storage and these points are given the most weightage by the error metric.

Performance of wavefunction methods

Before looking into the performance of different density functionals, we will briefly examine the performance of different wavefunction methods. Hartree Fock binding energies have

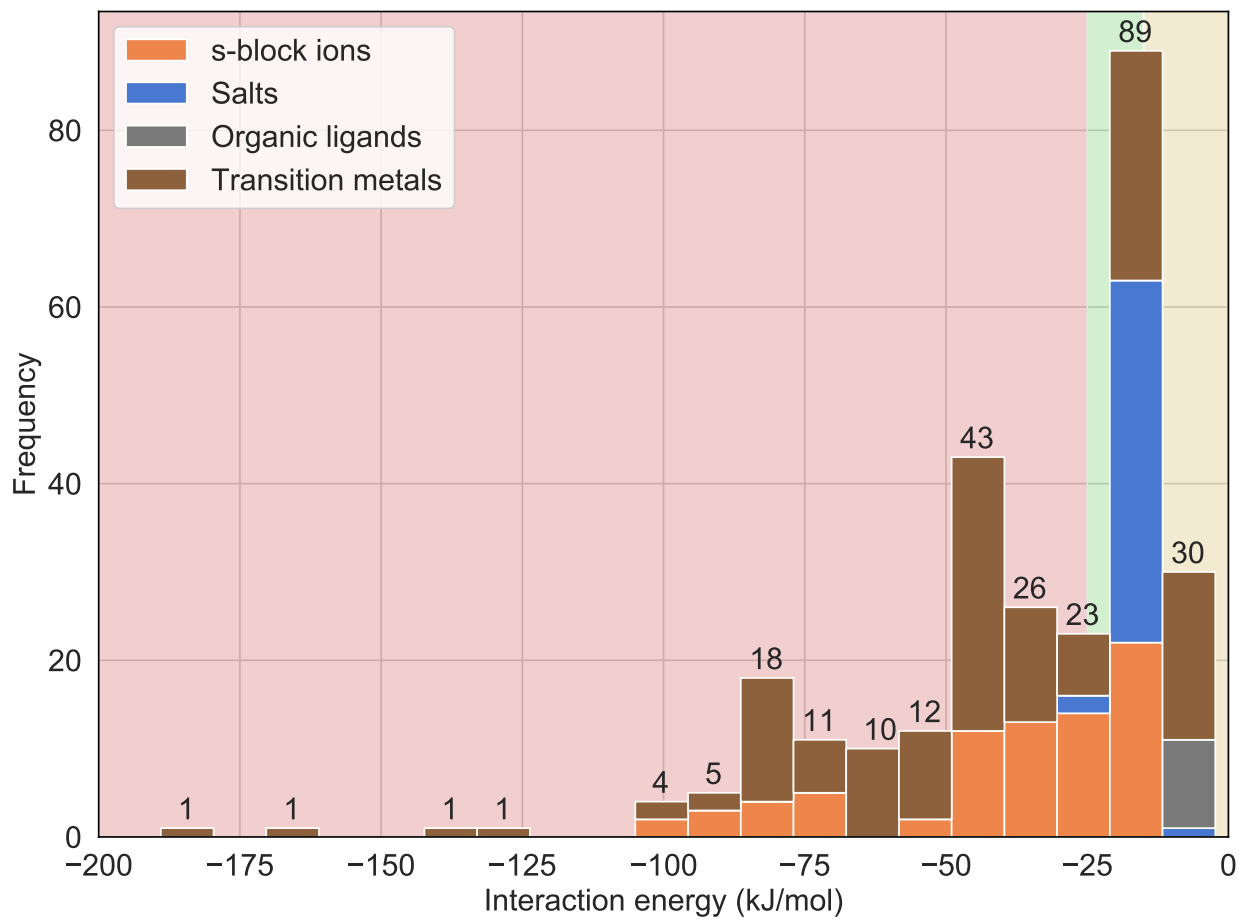


Figure 4: A figure showing the distribution of interaction energies for the whole H2Bind275 dataset.

a RegMAPE of 45% which highlights the importance of correlation energy for binding, as captured by coupled cluster theory. HF performs better than only the LDA density functionals. HF underbinds all the cases with a mean signed error of 19.6 kJ/mol. HF is unable to capture dispersion and predicts that all the dispersion-bound complexes like those in the organic ligands subset are unbound. MP2 at the quintuple-zeta quality basis set is able to capture most of the correlation binding energy and has a RegMAPE of only 5.9%. MP2 binding energies extrapolated to the complete basis set (CBS) limit perform slightly better with a RegMAPE of 5.2%. MP2 also slightly overbinds with a mean signed error of -1.8 kJ/mol which is consistent with the conventional wisdom in quantum chemistry that MP2 overestimates dispersion interactions.^{71,72}

Choice and overview of density functionals

While DFT is formally exact within the Born-Oppenheimer approximation, in practice, the exact form of the exchange-correlation functional remains unknown. As there is no systematic recipe for improving DFT, various groups all over the world have come up with multiple DFAs. As each of these approximations perform differently for various problems, in this section we characterize the performance of 55 DFAs for their ability to predict binding energies of H₂ to different binding substrates accurately. The 55 functionals were chosen based on different criteria. One of the criteria was their superior performance in non-covalent interaction energy databases.²² Density functionals were also chosen to represent distinct functional families being developed by leading research groups. We have also included some functionals that are frequently used in the H₂ storage modeling community. While there are different methods to classify density functionals, Perdew’s metaphorical Jacob’s ladder is the most popular one.⁷³ As one moves up the Jacob’s ladder from the Hartree world to the heaven of chemical accuracy, one can expect density functionals to get more and more accurate. However, this might not necessarily be true as increasing the degrees of freedom in density functionals as one moves up the Jacob’s ladder can also result in overfitting of parameters

and subsequently poor transferability. For further information about the functional forms of these density functionals, the number of parameters, and the datasets they were trained, we refer the reader to these comprehensive reviews of density functional development.^{22,23}

Table 3: A table showing all the density functional approximations benchmarked in this work classified by rung of the Jacob’s ladder.

Rung #	Rung name	Functionals
Rung 5	Double Hybrid	ω B97M(2), DSD-PBEPBE-D3(BJ), XYG3, B2PLYP-D3(BJ), PTPSS-D3(0), PBE0-DH, XYGJOS
Rung 4	Hybrid	B3LYP, B3LYP-D3(0), PBE0, PBE0-D3(BJ), MN15, TPSSh, TPSSh-D3(BJ), MVSh, SCAN0, M06, M06-2X, M06-2X-D3(0), revM06, ω B97M-V, ω B97X-D, ω B97X-D3, ω B97X-V, M11, revM11, HSE-HJS, MN12-SX
Rung 3	meta-GGA	TPSS, TPSS-D3(BJ), revTPSS, SCAN, SCAN-D3(BJ), MS2, MS2-D3(op), B97M-V, B97M-rV, M06-L, MN15-L, mBEEF
Rung 2	GGA	PBE, PBE-D3(0), PBE-D3(op), RPBE, revPBE, revPBE-D3(op), BLYP, BLYP-D3(op), PW91, GAM, B97-D3(0), B97-D3(BJ)
Rung 1	LDA	SPW92, SVWN5

Table (3) shows all the functionals chosen for benchmarking in this work. Rung one functionals, SVWN5⁷⁴ and SPW92,⁷⁵ contain Slater exchange and different parameterizations for correlation energy and depend only on electron density ρ . The 12 Generalized Gradient Approximation (GGA) density functionals chosen, depend on density and the gradient of density (ρ and $\nabla\rho$), can be classified into 6 families. The PBE family of density functionals represented in this paper consist of the original PBE density functional,⁷⁶ PBE-D3(0),⁷⁷ RPBE⁷⁸ and their revised counterparts revPBE⁷⁹ and revPBE-D3(op).⁸⁰ Other families represented include the BLYP family consisting of BLYP^{81,82} and BLYP-D3(op),⁸⁰ and the B97⁸³ family comprising B97-D3(0)⁷⁷ and B97-D3(BJ).⁸⁴ Other successful GGA functionals included are GAM,⁸⁵ PW91,⁸⁶ BP86-D3(BJ).^{81,84,87} Rung 3 functionals are called meta-GGA functionals and they depend on the density, gradient of density, and the kinetic energy density (ρ , $\nabla\rho$, and τ). Meta-GGAs tested in this study consist of the non-empirically developed TPSS,⁸⁸ TPSS-D3(BJ),⁸⁴ and revTPSS.⁸⁹ The more recently developed SCAN⁹⁰ and its dispersion-corrected counterpart (SCAN-D3(BJ)⁹¹) also belong to this rung. B97M-V

is a combinatorially optimized semi-local density functional with VV10 non-local correction developed by Mardirossian and Head-Gordon.⁹² B97M-rV⁹³ has the rVV10 non-local correction⁹⁴ refit to the parent B97M-V functional and can be efficiently implemented in periodic codes. The mBEEF functional developed by Bligaard and co-workers is expected to give superior results for surface science and catalysis problems.⁹⁵ Other meta-GGA functionals included in this study are the Minnesota functionals developed by Truhlar and co-workers (M06-L⁹⁶ and MN15-L⁹⁷), MS2,⁹⁸ and MS2-D3(op).⁸⁰ One of the biggest deficiencies of the semi-local density functionals (rung 1, 2, and 3) is self-interaction error which can be partially offset by adding some fraction of Hartree Fock exchange to the exchange-correlation functional.⁹⁹ Popular hybrid functionals are PBE0¹⁰⁰ and PBE0-D3(BJ)⁸⁴ from the PBE family and TPSSh¹⁰¹ and TPSSh-D3(BJ)⁸⁴ from the TPSS family and SCAN0¹⁰² from the SCAN family of density functionals. B3LYP¹⁰³ and B3LYP-D3(BJ)⁸⁴ are by far the most widely used density functionals today. Minnesota global hybrid functionals considered in this study are M06,¹⁰⁴ M06-2X,¹⁰⁴ M06-2X-D3(0),⁷⁷ revM06,¹⁰⁵ and MN15.¹⁰⁶ MVSh is another hybrid density functional developed by Perdew and co-workers evaluated for H₂ binding.¹⁰⁷ The aforementioned functionals, containing a fixed amount of exact exchange, only partially alleviate the problem of self-interaction error. A modified class of hybrid density functionals called range-separated hybrids present a more sophisticated approach to eliminating self-interaction error by treating exchange differently in long and short ranges.^{108,109} Short-range exchange is treated using both DFT exchange and exact exchange and only exact exchange is used in the long-range. ω B97X-D¹¹⁰ is a reparameterization of the original ω B97X¹¹¹ functional to include atom-atom dispersion and ω B97X-D3¹¹² is a further reparameterization to include Grimme’s D3 dispersion corrections.⁷⁷ ω B97X-V¹¹³ and ω B97M-V⁴⁰ are range-separated hybrid GGA and meta-GGA functionals derived from the combinatorial approach. These functionals have been shown to perform well for a wide range of chemical problems previously.²² M11¹¹⁴ and its recently published revised version revM11¹¹⁵ are other popular range-separated hybrids. Another strategy is to use Hartree Fock exchange in the short-

range and DFT exchange in the long-range. Such density functionals are amenable to usage in solid-state calculations, and are called screened exchange functionals. Two of such functionals, HSE-HJS^{116,117} and MN12-SX,¹¹⁸ are included in this study. The fifth rung of Jacob’s ladder consists of double hybrid density functionals which have some fraction of correlation energy from second order Møller-Plesset Perturbation Theory perturbation theory. Addition of a fraction of correlation from perturbation theory can be justified based on Görling-Levy perturbation theory.¹¹⁹ B2PLYP is the first density functional to use Kohn-Sham orbitals to compute a perturbation theory correction.¹²⁰ PBE0-DH is a non-empirical double-hybrid belonging to the PBE family.¹²¹ XYG3 double hybrid density functional introduced a new class of double hybrid density functionals which uses orbitals from a successful lower-rung density functional (B3LYP orbitals in the case of XYG3) to perform a single-shot computation of the exchange-correlation and PT2 energies.¹²² Other successful double hybrid density functionals following this approach are ω B97M(2)¹²³, the combinatorially-optimized double hybrid density functional using ω B97M-V orbitals and XYGJ-OS¹²⁴, the opposite-spin equivalent of XYG3. Other popular double hybrid density functionals like DSD-PBEPBE-D3(BJ)¹²⁵ and PTPSS-D3(0)¹²⁶ are also included for comparison.

Performance of density functional approximations

Fig. (5) shows that density functionals exhibit varied performance for H₂ binding applications. In general, the performance of the density functionals improves as we climb up Jacob’s ladder. However, this rule has many notable exceptions. Using RegMAPE as the error metric, we see that DSD-PBEPBE-D3(BJ), a spin-component-scaled double hybrid density functional with empirical dispersion correction provides the best performance with a RegMAPE value of 4.9%. DSD-PBEPBE-D3(BJ) also has the fourth least RMSE of 3.8 kJ/mol and both the error metrics show that this density functional is the best performing for H₂ storage as shown in Fig. (6) and Fig. (7). The second best performing functional is the combinatorially optimized range-separated hybrid GGA, ω B97X-V, which shows a

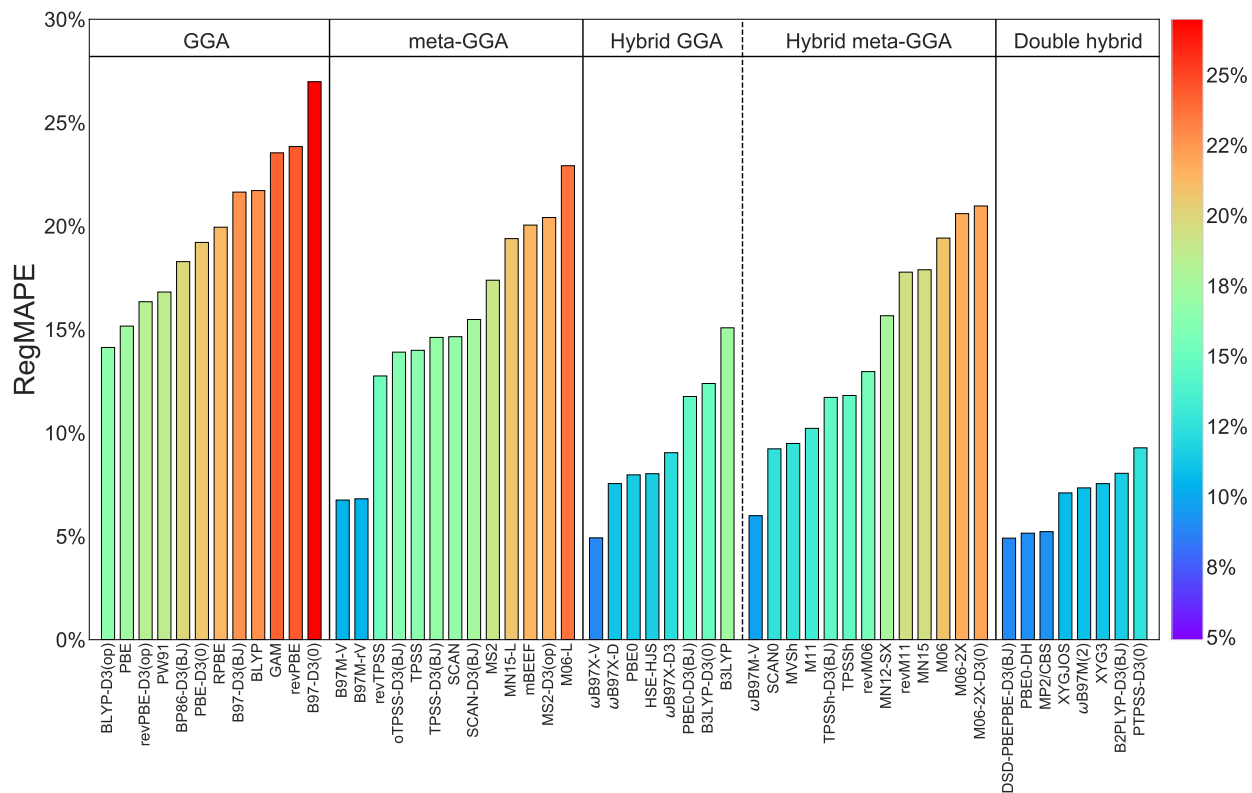


Figure 5: A figure showing the performance of the density functional approximations by rung of the Jacob’s ladder. The LDA functionals, SPW92 and SVWN5, have an error of 60.06% and 60.08% respectively, and have not been shown in this figure. MP2 interaction energies extrapolated to the complete basis set limit has also been shown for comparison.

Rank	s-block ions	Salts	Organic ligands	Transition metals	Total	DFA
1	1.5	1.3	2.0	4.1	3.1	PBE0-DH
2	1.4	0.7	0.2	4.5	3.3	ω B97X-V
3	1.0	0.8	0.3	5.1	3.7	ω B97M-V
4	0.8	1.0	0.2	5.2	3.8	DSD-PBEPBE-D3(BJ)
5	4.0	1.4	0.4	4.4	3.8	ω B97X-D
6	3.1	2.6	3.1	4.8	4.0	MVSh
7	2.3	2.2	2.7	5.3	4.1	PBE0
8	3.3	1.2	0.6	5.1	4.1	ω B97X-D3
9	2.4	2.0	2.6	5.4	4.2	HSE-HJS
10	1.7	2.9	0.9	5.5	4.2	XYG3
11	2.3	1.5	0.6	5.6	4.3	XYGJOS
12	0.9	1.0	0.4	6.4	4.6	PTPSS-D3(0)
13	1.7	2.3	0.4	6.4	4.8	ω B97M(2)
14	3.1	0.9	0.5	6.6	5.0	B2PLYP-D3(BJ)
15	2.2	4.4	4.5	6.4	5.2	TPSSh
16	3.7	1.1	0.4	6.6	5.2	PBE0-D3(BJ)
17	0.9	1.4	1.5	7.3	5.3	SCAN0
18	2.1	2.3	1.1	7.4	5.5	revM06
19	5.0	4.4	1.9	6.4	5.6	revM11
20	2.8	1.2	0.2	7.7	5.8	B3LYP-D3(0)
21	3.3	0.7	0.6	7.7	5.9	TPSSh-D3(BJ)
22	2.8	5.6	5.4	7.3	6.0	B3LYP
23	5.9	4.2	2.8	7.0	6.2	mBEEF
24	1.1	0.8	0.2	8.7	6.3	B97M-V
25	3.1	3.3	2.6	8.2	6.3	MN15
26	1.0	0.7	0.1	8.8	6.4	B97M-rV
27	2.0	3.4	3.9	8.6	6.5	revTPSS
28	2.8	2.2	1.1	8.9	6.6	σ TPSS-D3(BJ)
29	2.5	4.8	4.6	8.6	6.7	TPSS
30	5.0	4.3	4.2	8.1	6.7	MN15-L
31	4.1	1.6	0.4	9.3	7.1	revPBE-D3(op)
32	3.3	8.7	5.7	8.8	7.5	RPBE
33	3.9	2.5	0.8	10.1	7.7	BLYP-D3(op)
34	3.8	0.8	0.6	10.4	7.8	TPSS-D3(BJ)
35	4.3	10.0	7.1	8.5	7.8	revPBE
36	2.0	2.6	0.5	11.1	8.1	M11
37	1.8	3.1	0.5	11.1	8.2	B97-D3(BJ)
38	3.9	8.5	7.2	9.7	8.2	BLYP
39	3.7	1.2	0.7	11.6	8.6	MN12-SX
40	3.1	2.8	0.6	12.2	9.1	M06
41	3.6	2.5	2.7	12.4	9.3	PBE
42	2.2	3.2	0.4	12.9	9.5	B97-D3(0)
43	1.8	2.1	1.9	13.3	9.8	BP86-D3(BJ)
44	4.6	1.1	1.0	13.5	10.1	PBE-D3(0)
45	3.5	2.4	0.8	13.8	10.2	M06-L
46	4.6	1.6	1.8	13.6	10.2	PW91
47	1.6	2.8	0.4	14.7	10.8	M06-2X
48	1.7	2.9	0.7	14.7	10.8	M06-2X-D3(0)
49	1.3	1.2	1.6	15.0	10.9	SCAN
50	2.1	1.2	0.3	15.6	11.3	GAM
51	1.4	1.6	0.5	15.6	11.3	SCAN-D3(BJ)
52	2.9	1.5	0.9	15.5	11.4	MS2
53	3.5	2.4	1.1	16.0	11.7	MS2-D3(op)
54	11.7	10.2	3.9	39.6	29.6	SPW92
55	11.7	10.2	3.9	39.6	29.6	SVWN5

Double hybrid Hybrid meta-GGA GGA LDA

Figure 6: A figure showing the Root Mean Square Errors for each category of the dataset as well as the total RMSE. The functionals are arranged in ascending order of the total RMSE. The best performing density functional in each rung has been highlighted.

Rank	s-block ions	Salts	Organic ligands	Transition metals	Total	DFA
1	1.8	4.4	1.4	7.0	4.9	DSD-PBEPBE-D3(BJ)
2	2.2	3.5	1.3	7.1	4.9	ω B97X-V
3	1.9	5.9	16.6	5.9	5.2	PBE0-DH
4	1.2	3.8	2.0	9.5	6.0	ω B97M-V
5	2.7	3.7	1.3	10.2	6.8	B97M-V
6	2.5	3.9	0.7	10.4	6.8	B97M-rV
7	5.2	8.8	4.6	7.7	7.1	XYG-JOS
8	2.4	13.9	3.6	8.2	7.3	ω B97M(2)
9	2.6	16.8	7.4	7.4	7.5	XYG3
10	6.3	7.5	3.0	8.6	7.5	ω B97X-D
11	2.6	12.4	22.6	8.5	8.0	PBE0
12	2.7	11.4	21.6	8.9	8.0	HSE-HJS
13	5.6	4.2	3.7	10.8	8.0	B2PLYP-D3(BJ)
14	7.1	6.5	4.1	11.2	9.0	ω B97X-D3
15	2.1	8.1	12.1	13.2	9.2	SCAN0
16	2.7	5.6	3.1	14.3	9.3	PTPSS-D3(0)
17	9.8	13.5	26.1	6.9	9.5	MVSh
18	5.3	14.9	4.1	11.8	10.2	M11
19	6.2	3.4	4.4	17.7	11.7	TPSSh-D3(BJ)
20	7.8	6.5	2.8	16.1	11.8	PBE0-D3(BJ)
21	4.2	28.2	36.9	9.1	11.8	TPSSh
22	2.9	5.6	1.5	20.3	12.4	B3LYP-D3(0)
23	3.4	21.6	32.6	13.7	12.8	revTPSS
24	4.9	13.6	8.7	17.4	13.0	revM06
25	4.9	13.4	8.1	19.3	13.9	oTPSS-D3(BJ)
26	4.6	30.5	38.1	12.3	14.0	TPSS
27	5.4	13.1	6.7	19.7	14.1	BLYP-D3(op)
28	7.1	4.0	4.2	22.6	14.6	TPSS-D3(BJ)
29	3.7	7.2	13.5	22.9	14.7	SCAN
30	6.2	35.5	44.9	11.5	15.1	B3LYP
31	4.5	14.8	22.1	20.5	15.2	PBE
32	2.7	8.8	4.2	25.1	15.5	SCAN-D3(BJ)
33	6.4	6.6	4.4	24.2	15.7	MN12-SX
34	8.4	8.6	2.6	23.9	16.3	revPBE-D3(op)
35	7.3	8.6	14.2	24.6	16.8	PW91
36	5.7	8.9	7.4	26.9	17.4	MS2
37	12.8	28.2	15.7	17.4	17.8	revM11
38	7.8	20.2	21.1	22.4	17.9	MN15
39	5.1	13.0	15.3	26.9	18.3	BP86-D3(BJ)
40	8.1	6.3	8.3	29.9	19.2	PBE-D3(0)
41	11.9	24.0	34.9	20.9	19.4	MN15-L
42	6.4	15.3	3.7	28.7	19.4	M06
43	7.6	55.4	46.3	13.9	19.9	RPBE
44	17.3	27.5	23.3	19.0	20.0	mBEEF
45	8.2	14.8	9.0	29.4	20.4	MS2-D3(op)
46	3.2	16.5	2.9	32.4	20.6	M06-2X
47	3.4	17.5	4.9	32.5	21.0	M06-2X-D3(0)
48	2.7	18.6	3.3	34.0	21.6	B97-D3(BJ)
49	9.9	54.5	59.1	15.4	21.7	BLYP
50	6.1	13.3	6.0	36.0	22.9	M06-L
51	3.6	6.2	1.9	41.0	23.5	GAM
52	12.0	64.7	58.2	15.3	23.8	revPBE
53	6.2	16.1	3.0	43.1	27.0	B97-D3(0)
54	25.8	66.7	32.5	78.3	60.1	SPW92
55	25.8	66.7	32.4	78.3	60.1	SVWN5

Double hybrid
Hybrid
meta-GGA
GGA
LDA

Figure 7: A figure showing the RegMAPE for each category and the total RegMAPE of the dataset. The functionals are arranged in ascending order of the total RegMAPE. The best performing density functional in each rung has been highlighted.

RegMAPE of 4.9%, which is comparable to that of DSD-PBEPBE-D3(BJ). ω B97X-V also yields the lowest RMSE of 3.3 kJ/mol. It is followed by the non-empirical general purpose double hybrid density functional DSD-PBEPBE-D3(BJ) which shows an error of 5.2%. The 4th best performing density functional, ω B97M-V, has a gap of about 0.8% showing an error of 5.7%. ω B97M-V functional is the 3rd best performing density functional by RMSE and was also the best performing hybrid functional on a main group chemistry database of nearly 5000 data points.²² The B97M-V and the B97M-rV functionals closely follow with errors of 6.8%. This is especially interesting as B97M-V and B97M-rV are semi-local functionals which are much less expensive than hybrid functionals for both cluster and periodic computations.^{127–129} B97M-rV uses the rVV10 non-local functional, which allows efficient evaluation in plane wave basis codes.⁹⁴ Although these two functionals have a large RMSE of 6.3 and 6.4 kJ/mol, their erroneous predictions of binding energies seem to be largely concentrated in the region outside the interesting regime of -15 to -25 kJ/mol. Other double hybrid density functionals providing providing competitive performance are the XYGJOS, ω B97M(2), and XYG3 functionals. ω B97X-D, PBE0, and HSE-HJS hybrid functionals also show low RegMAPEs of 7.5%, 8.0%, and 8.0% respectively. MP2 interaction energy extrapolated to the complete basis set limit shows a low RegMAPE of 5.2% and is comparable to the performance of the best density functionals. This is further interesting given that double hybrid functionals are as expensive as MP2.

It is interesting to note that commonly used density functionals like B3LYP and PBE show very poor performance (ranked 30 and 31 respectively). The dispersion-corrected version of B3LYP, B3LYP-D3(0), shows some slight improvement in performance while that of PBE, PBE-D3(0) shows worse performance, jumping down 9 places. Effect of addition of dispersion correction is discussed in detail in a later subsection. Even newly developed functionals like SCAN show disappointing performance. The screened-exchange density functional HSE-HJS, which has been suggested for use in solid-state calculations, also shows excellent performance with a RegMAPE of 8.0% and RMSE of 4.2 kJ/mol. While MVSh

has a very low RMSE of 4.0 kJ/mol reflecting its good performance over the entire dataset weighted equally, its corresponding RegMAPE of 9.5% is not that impressive suggesting that it is not very suitable for usage in the interesting H₂ storage regime. XYG3, the first xDH density functional, shows comparable performance in terms of both RMSE and RegMAPE.

Performance by dataset category

While the goal of this work is to rank functionals based on their performance for the H₂ storage problem as represented by the entire H2Bind275 dataset, it would be useful to analyze their performances by chemical categories of the data in order to characterize the origin of errors. While the category errors are not designed to sum up to the total in Tables (6) and (7), they can be contrasted with each other in order to get a relative sense. Another error metric, the regularized maximum absolute percentage error, is shown in Table S6.

The errors from the transition metals category are the largest in both absolute (as indicated by RMSE) and relative error metrics (as indicated by RegMAPE). This is not surprising considering that the majority of the semi-empirical density functionals are trained on main-group molecular properties. The transferability of DFAs trained on main-group element properties to those of transition metals has been of significant interest in the DFA development community.¹³⁰ For the transition metal category, the PBE0-DH functional performs best with a RegMAPE of 5.9% and RMSE of 4.1 kJ/mol. MVSh performs the second best with a RegMAPE of 6.9% and is also the best performing hybrid functional. B97M-V is the best performing semi-local functional (as with the entire dataset).

The s-block ions category is second largest with 77 data points. This category, consisting of s-block monocations and dications, represent the ability of the density functionals to capture electrostatics and polarization interactions accurately. ω B97M-V outperforms all other functionals in this category with a RegMAPE of 1.2%. The second best performing functional is DSD-PBEPBE-D3(BJ) with a RegMAPE of 1.8% and this is closely followed by PBE0-DH. B97M-rV, a meta-GGA density functional, is the best performing semi-local

functional with a RegMAPE of 2.5%.

The organic ligands category is the smallest (only 10 data points), and tests the ability of density functionals to describe van der Waal’s interactions correctly. It is a little surprising to see that the local functional B97M-rV outperforms its hybrid and double hybrid counterparts. Evidently these functionals, with their VV10 non-local corrections, are well equipped to deal with such dispersion dominated interactions. The best performing hybrid is the ω B97X-V functional which appears 2nd in the ranking. PBE0-DH consistently underbinds all the 10 data points with a MSE of 2.0 kJ/mol leading to an RMSE of 2.0 kJ/mol and a quite large RegMAPE of 16.6%. This underestimation of dispersion reflects the fraction of PT2 which is substantiated by poorer performance of its hybrid and semi-local counterparts, PBE0 and PBE, which exhibit high RegMAPEs of 22.6% and 22.1% respectively. Upon addition of dispersion corrections via the PBE0-D3(BJ) and PBE-D3(0), their errors decrease to a mere 2.8% and 8.3% respectively.

The performance of DFAs in the salts category is also somewhat surprising because of the larger magnitude of errors in comparison to the other main group categories as the majority of the DFAs are trained on main-group chemistry properties. TPSSh-D3(BJ) is the best performing for the salts category with RegMAPE of 3.4% and RMSE of 0.7 kJ/mol. B97M-V is the best semi-local functional with a RegMAPE of 3.7% and RMSE of 0.8 kJ/mol. In this category, the best hybrid and semi-local functionals outperform the best double hybrid functional B2PLYP-D3(BJ).

Performance by interaction energy range

Hydrogen storage applications usually target materials that can bind H₂ with an interaction energy of -15 to -25 kJ/mol. As a consequence, binding moieties with interaction energies outside this range are less important but cannot be disregarded altogether as they might appear in modified forms or as secondary binding sites in storage materials. Our regularized error metric, RegMAPE is designed to weigh interactions in the favorable regime more than

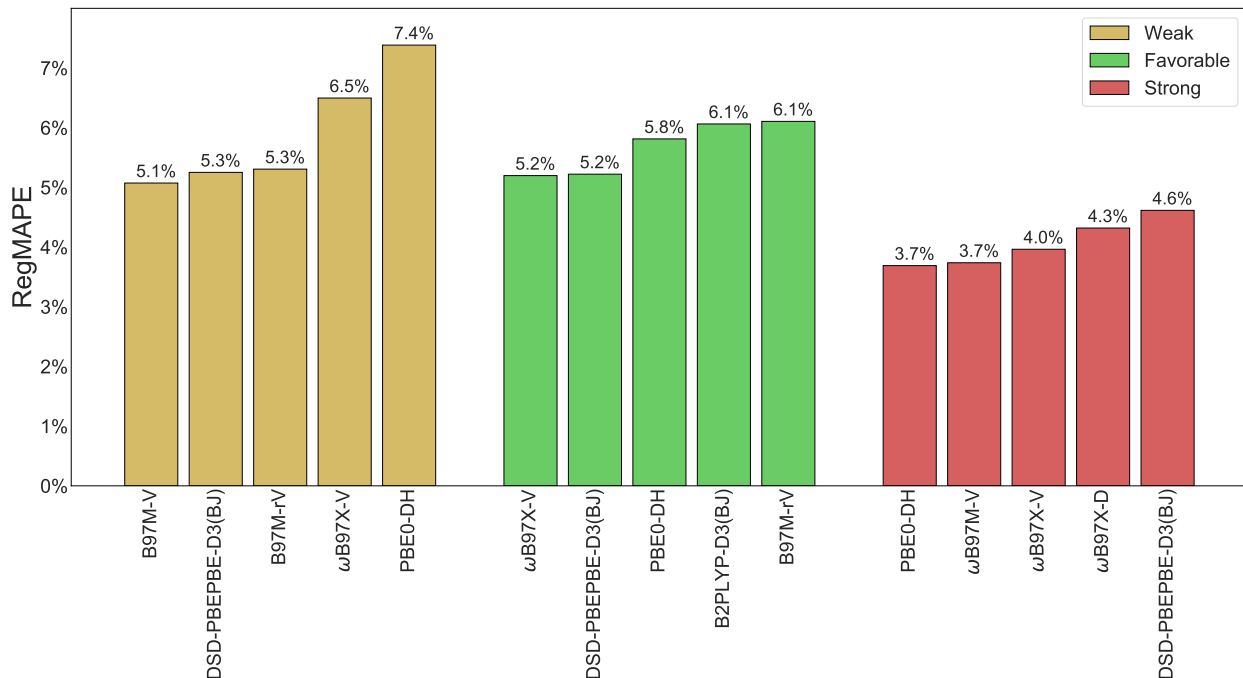


Figure 8: A plot showing the performance of the top five density functional approximations in the three interaction energy ranges relevant to H_2 binding applications: (a) Weak (less than -15 kJ/mol) (b) Favorable (-15 to -25 kJ/mol) (c) Strong (larger than -25 kJ/mol)

others. Semi-local functional like B97M-V outperforms others in the low interaction energy regime. The second best functional for this region is a double hybrid with D3(BJ) dispersion correction, DSD-PBEPBE-D3(BJ), with a RegMAPE of 5.3%. The best hybrid functional in this domain, ω B97X-V, has a RegMAPE of 6.5%. In the favorable regime where the data points have the most weight, the performance is reminiscent of the performance over the whole dataset with a few notable exceptions. ω B97X-V, DSD-PBEPBE-D3(BJ), and PBE0-DH appearing in the 1st, 2nd, and 3rd spots also appear in the top ten density functional list in the overall performance. This further illustrates that RegMAPE is performing as it was expected to - that is, it gives higher weights to data points within the favorable interaction energy regime. One notable exception is the double hybrid B2PLYP-D3(BJ) functional which is ranked 4th in the favorable regime with a RegMAPE of 6.1% but does not even appear in the top 10 density functional list due to large errors in the strong interaction energy regime. Fig. (8) shows smaller RegMAPE values for the strong regime as absolute

errors are used. PBE0-DH gives the best predictions in this regime with a RegMAPE of 3.7% and is closely followed by ω B97M-V and then by other range-separated hybrids like ω B97X-V and ω B97X-D. It is also interesting to note the poor performance of semi-local functionals. The best performing semi-local functional is MN15-L with a RegMAPE of 7.7%. Even functionals like B97M-V and B97M-rV, which provide very good performance in other categories, fail in this regime.

Performance by rung of Jacob’s ladder

Table 4: A table showing the best performing density functionals in each rung of the Jacob’s ladder along with their overall ranking, RegMAPE, and RMSE.

Rung	Rung name	Functional	Rank	RegMAPE (%)	RMSE (kJ/mol)
1	LDA	SPW92	54	60.1	29.6
2	GGA	BLYP-D3(op)	27	14.1	7.7
3	meta-GGA	B97M-V	5	6.8	6.3
4	Hybrid	ω B97X-V	2	4.9	3.3
5	Double hybrid	DSD-PBEPBE-D3(BJ)	1	4.9	3.8

Density functionals can be classified on the basis of Jacob’s ladder as was summarized in Table (3). It is generally expected that the density functionals perform better as one climbs the rungs of the Jacob’s ladder. Rung 1 of the Jacob’s ladder, consisting of density functionals that depend only on the density ρ , perform the worst among all the ones tested with a RegMAPE of 60.1%. The performance increases significantly upon moving from Rung 1 to Rung 2 with BLYP-D3(op) showing an error of 14.1% (RMSE of 7.7 kJ/mol). Other notable GGA functionals that show comparable performance are PBE and the revPBE-D3(op) functional. The revPBE-D3(op) also gives the lowest RMSE among the GGA functionals.

Upon moving up another rung from GGAs to meta-GGAs, the density functionals depend on the kinetic energy density (τ) in addition to the density and its gradient (ρ and $\nabla\rho$). The best meta-GGA functional, B97M-V, is also one of the best performing functionals of this work with a RegMAPE of 6.8%. This represents a significant improvement over the best GGA functional with a RegMAPE of 14.1%. However, in terms of RMSE, the root mean

square error of B97M-V is 6.3 kJ/mol. The performance of B97M-rV functional closely follows that of B97M-V, but the performance of meta-GGAs considerably worsens after this with the third best meta-GGA showing a RegMAPE of 12.8%, which is almost double that of B97M-V and B97M-rV. SCAN and its dispersion-corrected version, SCAN-D3(BJ), give larger errors of 14.7% and 15.5% respectively despite being recommended as one of the best performing meta-GGA density functionals in a comprehensive DFA performance assessment.²³ The mBEEF functionals, which is expected to give good performance for surface science and catalysis, performs very poorly with a RegMAPE of 20.0%, though it has a comparatively lower RMSE of 6.2 kJ/mol. While the best performing meta-GGA beats the best performing GGA functional, other meta-GGAs like SCAN, MS2, and MN15-L show poorer performance than the best GGA, BLYP-D3(op).

Hybrid functionals perform very well with ω B97X-V, showing the best performance with a RegMAPE of 4.9% (RMSE of 3.3 kJ/mol). It is closely followed by its hybrid meta-GGA counterpart, ω B97M-V, which shows a RegMAPE of 6.0% (RMSE of 3.7 kJ/mol). The third best performing meta-GGA functional is the long-range corrected ω B97X-D functional (RegMAPE of 7.5% and RMSE of 3.8 kJ/mol). Out of the top five hybrid functionals, four of them are range-separated, indicating their success relative to global hybrids having a constant fraction of exact exchange. The best performing Minnesota functional is M11 with a RegMAPE of 10.2% (RMSE of 8.1 kJ/mol). Other Minnesota hybrid meta-GGAs like revM11, MN15, M06, M06-2X, and M06-2X-D3(0) tested provide poor performance for H₂ binding energies.

Double hybrid functionals, with some fraction of MP2 correlation energy, consistently perform the best with five of the seven functionals tested appearing in the top 10 list of the best density functional approximations. Leading the pack is the DSD-PBEPBE-D3(BJ) functional with a RegMAPE of 4.9% and RMSE of 3.8 kJ/mol. This density functional also happens to be the best performing among the 55 functionals tested in this study. This is closely followed by the PBE0-DH functional. The combinatorially optimized ω B97M(2)

double hybrid does not outperform other functionals in rung 5 unlike its meta-GGA and hybrid counterparts. Even the worst performing double hybrid, PTPSS-D3(0), only has a RegMAPE of 9.3% (RMSE of 4.6 kJ/mol). Double hybrids, which contain some fraction of MP2 correlation energy, reflect the good performance of MP2 itself (RegMAPE of 5.9%).

Performance upon addition of HF exchange

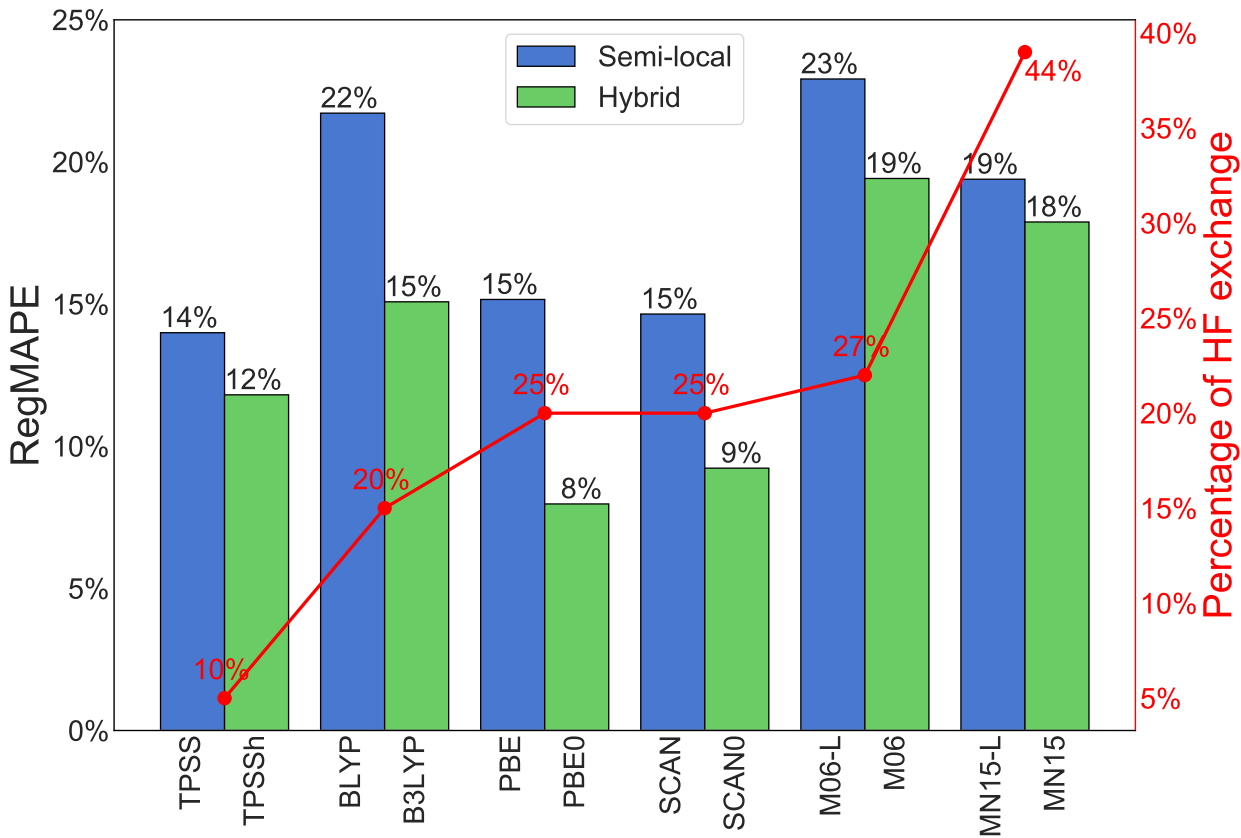


Figure 9: A graph showing the performance of density functional approximations with and without exact exchange. The right hand y-axis shows the percentage of HF exchange contained in each of the hybrid functionals.

Table S3 and Fig. (9) show the performance of density functional approximations belonging to the same family with and without exact exchange in order to quantify the effect of adding exact exchange to semi-local functionals. Addition of Hartree Fock exchange, also known as exact exchange, has been known to partially alleviate the problem of self-interaction error in density functionals. However, computation of exact exchange is the bottleneck in

the computation of the fock matrix for hybrid density functionals. In all the six families of densities functionals shown in Fig. (9), we see that addition of exact exchange improves the performance of the DFAs. All the hybrid density functionals considered in Fig. (9) are global hybrid functionals, meaning they contain a constant fraction of exact exchange for all inter-electronic distances. This is in contrast to range-separated hybrids which vary the amount of exact exchange with inter-electronic distance. The TPSSh functional contains a small amount of exact exchange (10%) and subsequently shows only a small improvement with RegMAPE going down by 2 percentage points. There is a significant improvement in the performance of BLYP, PBE, and SCAN functionals upon addition of a considerable amount of HF exchange. For example, the RegMAPE of PBE (15.2%) goes down by a factor of two upon addition of 25% exact exchange to make PBE0. However, in the case of the two Minnesota functionals examined, M06 family and MN15 family, we see that even addition of a large fraction of exact exchange does not improve the performance considerably. The M06-2X functional, which contains twice the amount of exact exchange (54%) in comparison to the M06 functional, also does not show significant improvement in H_2 binding energies with a RegMAPE of 20.6%. The additional computational cost in computing exact exchange is probably not justified for the minute improvement in the performance in the case of the Minnesota functionals. Range-separation represents a more successful strategy for combining HF exchange in the long range with DFT exchange in the short range. While the best global hybrid functional PBE0 ranks 11th, range-separated hybrids take the 2nd, 4th, and 10th spots. Another possible technique for range-separation is the screened exchange method, which uses HF exchange in the short range and DFT exchange in the long range. HSE-HJS and MN12-SX are screened exchange density functionals tested in this study. While there are no counterparts to compare against, we can see that the HSE-HJS functional performs reasonably well with a RegMAPE of 8.0%. On the other hand, the MN12-SX functional shows very poor performance.

Effect of dispersion corrections

Table 5: A table showing the Mean Signed Error(MSE), Root Mean Squared Error (RMSE), RegMAPE, and rank of the density functionals with and without dispersion correction.

No Dispersion correction					With Dispersion correction				
Functional	MSE	RMSE	RegMAPE	Rank	Functional	MSE	RMSE	RegMAPE	Rank
PBE	-4.9	9.3	15.2	31	PBE-D3(0)	-7.0	10.1	19.2	40
revPBE	4.3	7.8	23.8	52	revPBE-D3(op)	-3.6	7.1	16.3	34
BLYP	2.4	8.2	21.7	49	BLYP-D3(op)	-2.4	7.7	14.1	27
TPSS	-1.3	6.7	14.0	26	TPSS-D3(BJ)	-4.7	7.8	14.6	28
SCAN	-6.0	10.9	14.7	29	SCAN-D3(BJ)	-6.7	11.3	15.5	32
MS2	-7.3	11.4	17.4	36	MS2-D3(op)	-8.1	11.7	20.4	45
B3LYP	2.4	6.0	15.1	30	B3LYP-D3(0)	-1.1	5.8	12.4	22
PBE0	-1.2	4.1	8.0	11	PBE0-D3(BJ)	-3.6	5.2	11.8	20
TPSSh	-0.1	5.2	11.8	21	TPSSh-D3(BJ)	-3.3	5.9	11.7	19
M06-2X	-1.9	10.8	20.6	46	M06-2X-D3(0)	-2.0	10.8	21.0	47

In the absence of a strong electric field, dispersion is an important mechanism of interaction between H_2 and the binding site. These types of dispersion-dominated interactions are important in H_2 -organic linker interactions represented by the organic ligands category of H2Bind275. The inherent semi-local parameterization of DFAs make it difficult for them to capture long-range dispersion effects without additional corrections. Several methods have been introduced to calculate the effect of dispersion self-consistently and as a single-shot computation. Of the self-consistent methods introduced, the vdW-DF method (BEEF-vdW and optB88-vdW), the VV10 and rVV10 non-local correlation functional (ω B97M-V, ω B97X-V, B97M-V, and B97M-rV) have been used in different DFAs in this paper. The DFAs which have the VV10 correction for dispersion interactions are, in fact, the most successful ones as they incorporate the correct interaction physics via VV10 parameters that are set consistently with all other parameters related to semi-local XC and exact exchange to avoid double counting. Another inexpensive approach to incorporating the effect of dispersion is using Grimme’s empirical DFT-D suite of methods which is a damped atom-atom C_6 potential.^{77,131,132} Density functionals containing the original DFT-D3 scheme with the CHG-style damping function¹¹⁰ are suffixed by D3(0). The DFT-D3 scheme, combined with the damping function of Becke and Johnson are suffixed by D3(BJ).⁸⁴ Witte *et al.* further

generalized the Becke and Johnson damping function by optimizing the exponent of damping and this combination is termed D3(op).⁸⁰

In this section, we analyze the effect of addition of DFT-D type dispersion correction on the H₂ interaction energies. Dispersion corrections are always negative and will only make binding energies stronger. The effect of addition of dispersion to 10 DFAs is shown in Fig. S2 and Table (5). The addition of dispersion improves the performance of some DFAs while it worsens the performance of other DFAs. Addition of empirical dispersion to PBE, TPSS, SCAN, MS2, PBE0, and M06-2X makes their performance worse. In these cases, the parent density functional is already overbinding H₂(s) without dispersion corrections as shown by their negative Mean Signed Errors (MSE) in Table (5) and it is hence not very surprising to note that the dispersion-corrected results worsen. PBE, SCAN, and MS2 density functionals severely overbind with MSEs of -4.9, -6.0, and -7.3 kJ/mol. Addition of dispersion increases overbinding showing MSEs of -7.0, -6.7, and -8.1 kJ/mol. Addition of dispersion to PBE0 actually takes it from a top performing functional (ranked 11th) to a mediocre one (ranked 20th). Of the ten DFAs and their corresponding dispersion tails investigated in this section, MS2 is the most overbinding with a MSE of -7.3 kJ/mol, which only worsens slightly to -8.1 kJ/mol upon addition of dispersion correction. The correction is highly damped. A similar phenomenon is seen for M06-2X whose MSE increases only slightly from -1.9 to -2.0 kJ/mol. TPSSh is the only functional of the ten investigated that has neither an underbinding nor an overbinding problem with a MSE of -0.1 kJ/mol. Though addition of dispersion increases the MSE from -0.1 to -3.3 kJ/mol and RMSE from 5.2 to 5.9 kJ/mol, the corresponding RegMAPE changes slightly from 11.8% to 11.7% indicating that the dispersion corrections affects the interesting regime of H₂ binding only slightly.

Empirical dispersion corrections actually improve H₂ binding energy estimates for the revPBE, BLYP, and B3LYP functionals. Dispersion corrections enhance the performance of B3LYP from a RegMAPE of 15.1% to 12.4%. The parent density functional systematically underbinds with a MSE of 2.4 kJ/mol. Upon addition of dispersion, the B3LYP-D3(0) func-

tional systematically overbinds with a MSE of -1.1 kJ/mol. Addition of D3(op) correction to revPBE improves its performance from one of the worst performing functionals (ranked 52nd) to a mediocre performing functional (revPBE-D3(op) is ranked 34th). While the improvement in RMSE from 7.8 kJ/mol to 7.1 kJ/mol is not large, most improvement occurs in the interesting regime for H₂ binding, with RegMAPE improving significantly from 23.8% to 16.3%. Similarly, the dispersion-corrected BLYP functional, BLYP-D3(op), is the best performing GGA functional (ranked 26th) while its uncorrected counterpart is ranked 49th. Again, the improvement is concentrated in the interesting regime for H₂ storage materials.

Table 6: A table showing the performance of density functionals containing the non-local correlation vdW-DF-04 density functional of Lundqvist and Langreth relative to the performance of the best performing functionals for the spin unpolarized subset of the H2Bind275 dataset. OptB88-vDW and BEEF-vDW, density functionals containing vdW-DF-04 non-local correlation, exhibit poor performance.

Functional	RegMAPE	RMSE	Rank
ω B97M-V	2.7	3.1	1
ω B97X-V	2.8	2.6	2
DSD-PBEPBE-D3(BJ)	2.9	2.0	3
B97M-rV	3.6	4.1	4
B97M-V	3.6	4.1	5
optB88-vDW	9.7	5.9	37
BEEF-vDW	15.4	12.7	48

In this section, we briefly discuss the performance of density functional approximations containing the vdW-DF non-local correlation functional. This series of non-local functionals were initially developed to study layered materials, but has ever since been used to study a wide range of materials with dispersion interactions. The vdW-DF-04 non-local correlation functional¹³³ paired with optB88 exchange functional and LDA correlation functional (optB88-vdW)¹³⁴ has been widely used in modeling the hydrogen storage properties of different materials.^{135–138} However, the vdW-DF functional form has been defined only in the spin unpolarized form severely limiting its applicability. We have limited our analysis to two vdW-DF containing functionals: BEEF-vdW, a density functional within the bayesian error estimation framework, and optB88-vdW, containing the B88 exchange functional with

parameters optimized to best reproduce the interaction energies of the S22 dataset. We find that both these functionals show poor performance in terms of all error metrics used. The optB88-vdW and BEEF-vdW functionals show a RegMAPE of 9.7% and 15.4% ranking 37th and 48th respectively. The magnitude of this error should be contrasted to ω B97M-V, the best performing DFA for this spin unpolarized subset which gives a RegMAPE of 2.7%. This subset also contains the easier portion of the dataset as the errors for this subset are much smaller than those for the entire dataset. For example, the ω B97M-V functional gives an error of 6.0% for the entire dataset but gives only an error of 2.7% for this subset. This further exacerbates the failure of the vdW-DF functionals to appropriately capture the physics of interaction between H₂ and binding moieties. Both DFAs show systematic underbinding suggesting that dispersion interactions have not been captured completely. We also find that the large magnitude of error does not originate from a couple of outliers, but from their systematic inability to describe interaction physics correctly in a wide range of chemical species.

Top five best performing density functionals

In this section, we will attempt to understand the sources of error in the top five best performing density functionals in the entire H2Bind275 dataset: DSD-PBEPBE-D3(BJ), ω B97X-V, PBE0-DH, ω B97M-V, and B97M-V. Having identified these functionals for overall good performance for H₂ binding applications, it will be very informative to understand the origin of errors in these functionals and hence the shortcomings of currently available density functional approximations. A systematic understanding of the failure of the best density functionals could provide new avenues for development of better density functional approximations for H₂ storage and other applications. The top five functionals chosen also cover rungs 3–5 of Jacobs ladder with two double hybrids, two hybrids, and one semi-local meta-GGA. Each of these categories is also representative of the different costs associated with evaluating the density functionals with double hybrids being the most expensive, fol-

lowed by hybrids, and lastly by semi-local functionals. Reduction of the computational cost of hybrid functionals to that of semi-local functionals is an active area of research.^{139–141}

The largest contributors of error for the DSD-PBEPBE-D3(BJ) functional are the Ti^+ and Sc^+ species. Other species like Zn^+ , Cr^+ , and CaCl_2 are also leading sources of error. For the $\omega\text{B97X-V}$ functional, most errors come from transition metal species with predictions incorrect by about 46% for some Ti^+ species. Zn^+ and Fe^+ are some other species exhibiting large errors from 10% to 25%. The PBE0-DH also fails to predict accurate interaction energies for the Ti^+ species making errors of up to 56%. Zn^+ and Fe^+ are some difficult species for the the PBE0-DH functional. PBE0-DH also fails to predict the interaction energies with organic species accurately because of the lack of dispersion corrections as noted earlier. It is rather unsatisfying to see the failure of PBE0-DH for organic species, which are supposed to be easy problems for density functional approximations. However, a simple addition of Grimme-type dispersion correction cannot fix this issue as PBE0-DH systematically overbinds (MSE of -0.7 kJ/mol). $\omega\text{B97M-V}$ is the 4th best performing density functional, and its major contributors of error are Ti^+ , Zn^+ , and Fe^+ species. B97M-V also incorrectly predicts the interaction energies of Ti^+ species by about 66%. There are a few common denominators among the major contributors of error for the top five best performing functionals. These species mostly belong to the transition metal category. This is rather expected as majority of them are trained on main group chemistry properties. While some density functionals like MN15 have been trained on transition metal properties,¹⁰⁶ it is interesting to see density functionals like $\omega\text{B97M-V}$ and B97M-rV, which were trained on main-group chemistry properties providing comparable performance to that of MN15 for transition metal properties.¹³⁰

Semi-local and hybrid DFT calculations scale as the third power in the size of the one-particle basis set. Double hybrids, with the density fitting approximation for the MP2 piece, scale as the fifth power of the size of the basis set. While this scaling is much more favorable than that of CCSD(T), it limits the applicability of DFAs to systems of larger sizes. In the

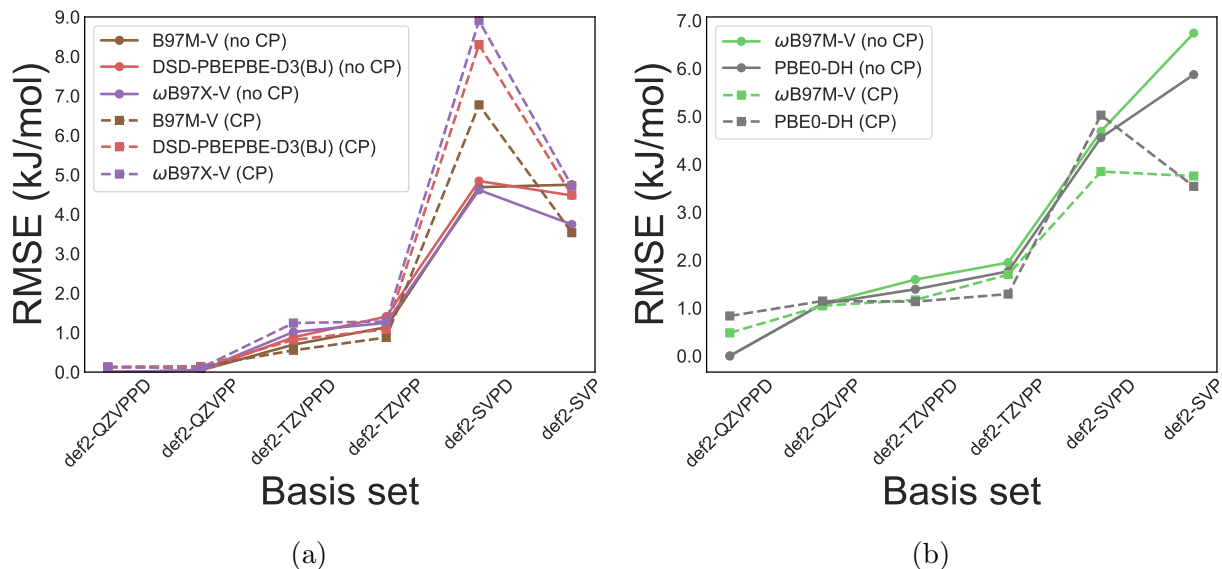


Figure 10: (a) A figure showing the errors in the counterpoise corrected and uncorrected interaction energies for ω B97X-V, ω B97M-V, and B97M-V with counterpoise corrected def2-QZVPPD interaction energies as the reference. (b) A figure showing the errors in the counterpoise corrected and uncorrected interaction energies for DSD-PBEPBE-D3(BJ), and PBE0-DH with counterpoise corrected def2-QZVPPD interaction energies as the reference.

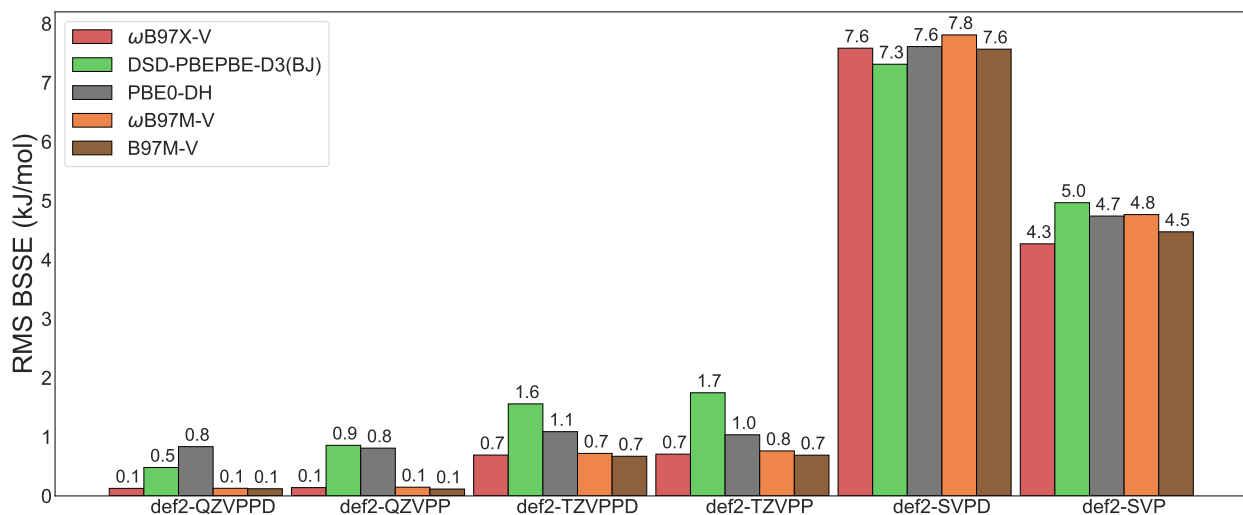


Figure 11: A figure showing the basis set superposition error for the top five best performing DFAs for different Karlsruhe basis sets.

context of using DFAs to screen potential H₂ adsorption materials, it can limit the number of screenings possible in a given period of time. All interaction energies computations using finite basis sets suffer from two distinct kinds of error: Basis Set Superposition Error (BSSE) and Basis Set Incompleteness Error (BSIE). In finite basis set computations, these two errors may partially cancel. Basis set superposition error can be reduced by the counterpoise correction.¹⁴²

Fig. (10) shows the errors in finite basis set interaction energy calculations for the top five DFAs in this study. All calculations were performed only on the vertical interaction energy subset as performing basis set superposition error corrections to adiabatic interaction energies is not straightforward. All the errors are computed with respect to the counterpoise corrected def2-QZVPPD interaction energy for the respective DFA so as to isolate the basis set errors from the DFA errors. BSSE decreases with increase in the basis set size for all the DFAs except for def2-SVPD/def2-SVP. In the case of the small def2-SVPD basis set, monomers can hugely benefit by borrowing the diffuse functions belonging to the other monomers. While this is possible even in the def2-TZVPPD and def2-QZVPPD case, the monomer’s own basis sets are large enough that they do not gain much from borrowing a neighbor’s diffuse function. Note the large magnitude of BSSE for the double hybrid density functionals in triple and quadruple-zeta basis sets in comparison to other DFAs. Even in the large quadruple-zeta def2-QZVPPD basis set, the double hybrids DSD-PBEPBE-D3(BJ) and PBE0-DH have a BSSE of 0.5 and 0.8 kJ/mol, while the BSSE of non double hybrid functionals is limited to 0.1 kJ/mol. This can be attributed to the fact that MP2 component in the double hybrids converges slowly with the basis set size.

Upon reducing the size of the basis set from def2-QZVPPD, both BSSE and BSIE cause overestimation and underestimation of interaction energies respectively. In the def2-QZVPP basis set, the counterpoise corrected and counterpoise uncorrected interaction energies show performance comparable to that of def2-QZVPPD with counterpoise corrected energies being slightly better. In the def2-TZVPPD basis set, the counterpoise uncorrected interaction

energies perform slightly better. Counterpoise uncorrected interaction energies in the def2-TZVPP basis are the best compromise between accuracy and cost with errors of about 1 kJ/mol for the semi-local and hybrid functionals and 1.5 kJ/mol for the double hybrids. The opposite trend is seen in the def2-SVPD basis set with counterpoise corrected energies being better than their uncorrected counterparts. The error cancellation is much more effective for double hybrids in this small basis set than the semi-local or hybrid functionals in which the BSSE dominates, leading to a systematic underbinding in the counterpoise uncorrected case. The error cancellation is even more effective in the def2-SVP case with RMSE of 3.5 to 4.5 kJ/mol.

Conclusions

In the search for improved H₂ storage materials, density functional approximations could potentially be used to screen and simulate adsorption frameworks. In this work, we have created a dataset of 275 different chemical moieties, binding one or multiple H₂s to capture the different physical and chemical modes of hydrogen activation in various adsorbent paradigms. We have compiled highly accurate reference interaction energies for the dataset using coupled cluster theory with singles, doubles, and perturbative triples with the focal point analysis scheme. We have assessed the performance of 55 density functional approximations from all rungs of the Jacob’s ladder using an error metric specifically designed to give larger weight to interaction energies in the range of -15 to -25 kJ/mol. We have examined the effect of exact exchange and empirical dispersion corrections on the performance of density functionals. We have identified problematic cases for density functionals, and have recommended efficient techniques to predict hydrogen interaction binding energies.

Of the 55 DFAs assessed in this study, we have identified five density functionals for providing the best performance. These five functionals are ω B97X-V and ω B97M-V in the hybrids category, DSD-PBEPBE-D3(BJ) and PBE0-DH in the double hybrids category, and B97M-V in the semi-local meta-GGA category. DSD-PBEPBE-D3(BJ) performs the best

over the 275 data points with an error of 4.9%. B97M-V is the best performing semi-local functional with a error of 6.8%. The B97M-rV functional also provides equally competitive performance, and with the rVV10 modification, it can also be efficiently used in periodic codes. Modern density functional approximations fail to accurately predict interaction energies of transition metal containing systems causing the biggest errors in that category. The best performing DFA at each rung of the Jacob’s ladder surpasses the best DFA from the previous rung. We have also identified that the addition of the exact exchange usually helps with the performance of the density functionals. However, there is no systematic improvement in performance with the fraction of exact exchange present in DFAs. Addition of empirical dispersion correction can immensely benefit systematically underbinding DFAs like revPBE, BLYP, and B3LYP. However, empirical dispersion corrections should be utilized with caution as they will only worsen the performance if the parent DFA is already overbinding. We have also illustrated the interplay between the two major sources of error associated with using finite basis sets: basis set superposition error and basis set incompleteness error. Taking advantage of the error cancellation between these two sources, we have shown that using def2-TZVPP basis without counterpoise corrections provides a good compromise between accuracy and cost.

With the identification of density functional approximations that can accurately predict interaction energies of H_2 with a wide variety of binding moieties, we have expanded the set of in silico tools that can accelerate the discovery and validation of new hydrogen storage materials. These density functionals can be used to screen potential binding sites in a high-throughput fashion or can be used to train framework-specific force fields for use in molecular dynamics and/or Monte Carlo simulations. The H2Bind275 dataset contains only geometries in which H_2 is at the minimum of the potential energy curve with respect to the binding moiety, thereby maximizing the interaction energy. It would be useful for the H_2 storage community to see if these conclusions are extensible to other points on the potential energy curve using the strategies similar to the S22x5¹⁴³ and S66x8 dataset.¹⁴⁴ One could also

conceive of similar assessments for properties like infrared frequencies. It would be useful to assess the performance of the best performing density functionals found in this work on real-life H₂ storage materials like MOFs, given the availability of highly accurate reference interaction energies. This will require careful consideration of the zero-point vibrational energies. Finally, future density functionals can be evaluated on this dataset to assess their suitability for hydrogen storage applications, or as part of testing functional performance for non-covalent interactions.

Supplementary Information

The geometries of all the species used in the H2Bind275 dataset and details necessary for reproducing all the data are provided in the supplementary information (geometries.zip). The ab initio reference interaction energies along with component-wise breakdown and DFT interaction energies for the 55 functionals are also provided (Supplementary_information.xlsx). The performance of the density functionals included in this work on the MGCDB84 is provided in the supplementary information for comparison. Another error metric, regularized maximum absolute percentage error, is also included.

Acknowledgements

We thank Dr. Romit Chakraborty for suggesting that we include monocationic transition metal containing species in our dataset. We thank Dr. Ehud Tsivion for providing us some model complexes for the H2Bind275 dataset. We thank Dr. Narbe Mardirossian for sharing the DFA interaction energies for the A24 dataset and ranking of density functionals over the MGCDB84 database, Dr. Joonho Lee for insightful discussions about the multireference character of the transition metal species, and Dr. Yuezhi Mao for helpful discussions about using Q-Chem. This work was supported by the Hydrogen Materials – Advanced Research Consortium (HyMARC), established as part of the Energy Materials Network under the U. S. Department of Energy, Office of Energy Efficiency and Renewable Energy, Fuel Cell

Technologies Office, under Contract Number DE-AC02-05CH11231. The following author declares competing financial interest. M. H. G. is a part owner of Q-Chem, Inc.

References

- (1) Allendorf, M. D.; Hulvey, Z.; Gennett, T.; Ahmed, A.; Autrey, T.; Camp, J.; Seon Cho, E.; Furukawa, H.; Haranczyk, M.; Head-Gordon, M.; Jeong, S.; Karkamkar, A.; Liu, D. J.; Long, J. R.; Meihaus, K. R.; Nayyar, I. H.; Nazarov, R.; Siegel, D. J.; Stavila, V.; Urban, J. J.; Veccham, S. P.; Wood, B. C. An assessment of strategies for the development of solid-state adsorbents for vehicular hydrogen storage. *Energy Environ. Sci.* **2018**, *11*, 2784–2812.
- (2) Chen, Z.; Li, P.; Anderson, R.; Wang, X.; Zhang, X.; Robison, L.; Redfern, L. R.; Moribe, S.; Islamoglu, T.; Gómez-Gualdrón, D. A., et al. Balancing volumetric and gravimetric uptake in highly porous materials for clean energy. *Science* **2020**, *368*, 297–303.
- (3) Chen, B.; Eddaoudi, M.; Reineke, T. M.; Kampf, J. W.; O’Keeffe, M.; Yaghi, O. M. Cu₂(ATC)6H₂O: Design of Open Metal Sites in Porous MetalOrganic Crystals (ATC: 1,3,5,7-Adamantane Tetracarboxylate). *J. Am. Chem. Soc.* **2000**, *122*, 11559–11560.
- (4) Kapelewski, M. T.; Geier, S. J.; Hudson, M. R.; Stck, D.; Mason, J. A.; Nelson, J. N.; Xiao, D. J.; Hulvey, Z.; Gilmour, E.; FitzGerald, S. A.; Head-Gordon, M.; Brown, C. M.; Long, J. R. M₂(m-dobdc) (M = Mg, Mn, Fe, Co, Ni) MetalOrganic Frameworks Exhibiting Increased Charge Density and Enhanced H₂ Binding at the Open Metal Sites. *J. Am. Chem. Soc.* **2014**, *136*, 12119–12129.
- (5) Dincă, M.; Han, W. S.; Liu, Y.; Dailly, A.; Brown, C. M.; Long, J. R. Observation of Cu₂+–H₂ Interactions in a Fully Desolvated Sodalite-Type Metal–Organic Framework. *Angew. Chem., Int. Ed.* **2007**, *46*, 1419–1422.
- (6) Jackson, K. T.; Reich, T. E.; El-Kaderi, H. M. Targeted synthesis of a porous borazine-linked covalent organic framework. *Chem. Commun.* **2012**, *48*, 8823–8825.

- (7) Zhu, S.; Li, T. Hydrogenation-assisted graphene origami and its application in programmable molecular mass uptake, storage, and release. *ACS Nano* **2014**, *8*, 2864–2872.
- (8) Kim, T. H.; Bae, J.; Lee, T. H.; Hwang, J.; Jung, J. H.; Kim, D. K.; Lee, J. S.; Kim, D. O.; Lee, Y. H.; Ihm, J. Room-temperature hydrogen storage via two-dimensional potential well in mesoporous graphene oxide. *Nano Energy* **2016**, *27*, 402–411.
- (9) Burrell, J. W.; Gadipelli, S.; Ford, J.; Simmons, J. M.; Zhou, W.; Yildirim, T. Graphene oxide framework materials: theoretical predictions and experimental results. *Angew. Chem., Int. Ed.* **2010**, *49*, 8902–8904.
- (10) Teichmann, D.; Arlt, W.; Wasserscheid, P.; Freymann, R. A future energy supply based on Liquid Organic Hydrogen Carriers (LOHC). *Energy Environ. Sci.* **2011**, *4*, 2767–2773.
- (11) Garrone, E.; Bonelli, B.; Otero Areán, C. Enthalpy-entropy correlation for hydrogen adsorption on zeolites. *Chem. Phys. Lett.* **2008**, *456*, 68–70.
- (12) Palomino, G. T.; Cabello, C. P.; Areán, C. O. Enthalpy-entropy correlation for hydrogen adsorption on MOFs: Variable-temperature FTIR study of hydrogen adsorption on MIL-100(Cr) and MIL-101(Cr). *Eur. J. Inorg. Chem.* **2011**, *100*, 1703–1708.
- (13) Areán, C. O.; Chavan, S.; Cabello, C. P.; Garrone, E.; Palomino, G. T. Thermodynamics of Hydrogen Adsorption on Metal-Organic Frameworks. *ChemPhysChem* **2010**, *11*, 3237–3242.
- (14) Řezáč, J.; Hobza, P. Benchmark Calculations of Interaction Energies in Noncovalent Complexes and Their Applications. *Chem. Rev.* **2016**, *116*, 5038–5071.

- (15) Parr, R.; Weitao, Y. *Density-Functional Theory of Atoms and Molecules*; International Series of Monographs on Chemistry; Oxford University Press, 1994.
- (16) Tsvion, E.; Mason, J. A.; Gonzalez, M. I.; Long, J. R.; Head-Gordon, M. A computational study of CH₄ storage in porous framework materials with metalated linkers: connecting the atomistic character of CH₄ binding sites to usable capacity. *Chem. Sci.* **2016**, *7*, 4503–4518.
- (17) Tsvion, E.; Veccham, S. P.; Head-Gordon, M. High-Temperature Hydrogen Storage of Multiple Molecules: Theoretical Insights from Metalated Catechols. *ChemPhysChem* **2017**, *18*, 184–188.
- (18) Colón, Y. J.; Snurr, R. Q. High-throughput computational screening of metal–organic frameworks. *Chem. Soc. Rev.* **2014**, *43*, 5735–5749.
- (19) Zong, S.; Zhang, Y.; Lu, N.; Ma, P.; Wang, J.; Shi, X.-R. A DFT Screening of M-HKUST-1 MOFs for Nitrogen-Containing Compounds Adsorption. *Nanomaterials* **2018**, *8*, 958.
- (20) Campbell, C.; Ferreiro-Rangel, C. A.; Fischer, M.; Gomes, J. R.; Jorge, M. A transferable model for adsorption in MOFs with unsaturated metal sites. *J. Phys. Chem. C* **2017**, *121*, 441–458.
- (21) Lee, K.; Howe, J. D.; Lin, L.-C.; Smit, B.; Neaton, J. B. Small-molecule adsorption in open-site metal–organic frameworks: a systematic density functional theory study for rational design. *Chem. Mater.* **2015**, *27*, 668–678.
- (22) Mardirossian, N.; Head-Gordon, M. Thirty years of density functional theory in computational chemistry: an overview and extensive assessment of 200 density functionals. *Mol. Phys.* **2017**, *8976*, 1–58.

- (23) Goerigk, L.; Hansen, A.; Bauer, C.; Ehrlich, S.; Najibi, A.; Grimme, S. A look at the density functional theory zoo with the advanced GMTKN55 database for general main group thermochemistry, kinetics and noncovalent interactions. *Phys. Chem. Chem. Phys.* **2017**, *19*, 32184–32215.
- (24) Hait, D.; Head-Gordon, M. How Accurate Is Density Functional Theory at Predicting Dipole Moments? An Assessment Using a New Database of 200 Benchmark Values. *J. Chem. Theory Comput.* **2018**, *14*, 1969–1981.
- (25) Hait, D.; Head-Gordon, M. How accurate are static polarizability predictions from density functional theory? An assessment over 132 species at equilibrium geometry. *Phys. Chem. Chem. Phys.* **2018**, *20*, 19800–19810.
- (26) Fetisov, E. O.; Shah, M. S.; Long, J. R.; Tsapatsis, M.; Siepmann, J. I. First principles Monte Carlo simulations of unary and binary adsorption: CO₂, N₂, and H₂O in Mg-MOF-74. *Chem. Commun.* **2018**, *54*, 10816–10819.
- (27) Sumida, K.; Stck, D.; Mino, L.; Chai, J.-D.; Bloch, E. D.; Zavorotynska, O.; Murray, L. J.; Dinc, M.; Chavan, S.; Bordiga, S.; Head-Gordon, M.; Long, J. R. Impact of Metal and Anion Substitutions on the Hydrogen Storage Properties of M-BTT MetalOrganic Frameworks. *J. Am. Chem. Soc.* **2013**, *135*, 1083–1091, PMID: 23244036.
- (28) Tsivion, E.; Long, J. R.; Head-Gordon, M. Hydrogen physisorption on metal-organic framework linkers and metalated linkers: A computational study of the factors that control binding strength. *J. Am. Chem. Soc.* **2014**, *136*, 17827–17835.
- (29) Shao, Y.; Gan, Z.; Epifanovsky, E.; Gilbert, A. T.; Wormit, M.; Kussmann, J.; Lange, A. W.; Behn, A.; Deng, J.; Feng, X.; Ghosh, D.; Goldey, M.; Horn, P. R.; Jacobson, L. D.; Kaliman, I.; Khaliullin, R. Z.; Kus, T.; Landau, A.; Liu, J.; Proynov, E. I.; Rhee, Y. M.; Richard, R. M.; Rohrdanz, M. A.; Steele, R. P.; Sundstrom, E. J.; Woodcock, H. L.; Zimmerman, P. M.; Zuev, D.; Albrecht, B.; Alguire, E.; Austin, B.; Be-

ran, G. J.; Bernard, Y. A.; Berquist, E.; Brandhorst, K.; Bravaya, K. B.; Brown, S. T.; Casanova, D.; Chang, C. M.; Chen, Y.; Chien, S. H.; Closser, K. D.; Crittenden, D. L.; Diedenhofen, M.; Distasio, R. A.; Do, H.; Dutoi, A. D.; Edgar, R. G.; Fatehi, S.; Fusti-Molnar, L.; Ghysels, A.; Golubeva-Zadorozhnaya, A.; Gomes, J.; Hanson-Heine, M. W.; Harbach, P. H.; Hauser, A. W.; Hohenstein, E. G.; Holden, Z. C.; Jagau, T. C.; Ji, H.; Kaduk, B.; Khistyayev, K.; Kim, J.; Kim, J.; King, R. A.; Klunzinger, P.; Kosenkov, D.; Kowalczyk, T.; Krauter, C. M.; Lao, K. U.; Laurent, A. D.; Lawler, K. V.; Levchenko, S. V.; Lin, C. Y.; Liu, F.; Livshits, E.; Lochan, R. C.; Luenser, A.; Manohar, P.; Manzer, S. F.; Mao, S. P.; Mardirossian, N.; Marenich, A. V.; Maurer, S. A.; Mayhall, N. J.; Neuscammann, E.; Oana, C. M.; Olivares-Amaya, R.; Oneill, D. P.; Parkhill, J. A.; Perrine, T. M.; Peverati, R.; Prociuk, A.; Rehn, D. R.; Rosta, E.; Russ, N. J.; Sharada, S. M.; Sharma, S.; Small, D. W.; Sodt, A.; Stein, T.; Stück, D.; Su, Y. C.; Thom, A. J.; Tsuchimochi, T.; Vanovschi, V.; Vogt, L.; Vydrov, O.; Wang, T.; Watson, M. A.; Wenzel, J.; White, A.; Williams, C. F.; Yang, J.; Yeganeh, S.; Yost, S. R.; You, Z. Q.; Zhang, I. Y.; Zhang, X.; Zhao, Y.; Brooks, B. R.; Chan, G. K.; Chipman, D. M.; Cramer, C. J.; Goddard, W. A.; Gordon, M. S.; Hehre, W. J.; Klamt, A.; Schaefer, H. F.; Schmidt, M. W.; Sherrill, C. D.; Truhlar, D. G.; Warshel, A.; Xu, X.; Aspuru-Guzik, A.; Baer, R.; Bell, A. T.; Besley, N. A.; Chai, J. D.; Dreuw, A.; Dunietz, B. D.; Furlani, T. R.; Gwaltney, S. R.; Hsu, C. P.; Jung, Y.; Kong, J.; Lambrecht, D. S.; Liang, W.; Ochsenfeld, C.; Rassolov, V. A.; Slipchenko, L. V.; Subotnik, J. E.; Van Voorhis, T.; Herbert, J. M.; Krylov, A. I.; Gill, P. M.; Head-Gordon, M. Advances in molecular quantum chemistry contained in the Q-Chem 4 program package. *Mol. Phys.* **2015**, *113*, 184–215.

(30) Kállay, M.; Surján, P. R. Higher excitations in coupled-cluster theory. *J. Chem. Phys.* **2001**, *115*, 2945–2954.

(31) Rolik, Z.; Szegedy, L.; Ladjánszki, I.; Ladóczki, B.; Kállay, M. An efficient linear-

- scaling CCSD (T) method based on local natural orbitals. *J. Chem. Phys.* **2013**, *139*, 094105.
- (32) Kállay, M.; Rolik, Z.; Csontos, J.; Ladjánszki, I.; Szegedy, L.; Ladóczki, B.; Samu, G.; Petrov, K.; Farkas, M.; Nagy, P., et al. MRCC, a quantum chemical program suite. URL: <http://www.mrcc.hu>, accessed August 26th **2016**,
- (33) Hobza, P.; Šponer, J. Structure, energetics, and dynamics of the nucleic acid base pairs: nonempirical ab initio calculations. *Chem. Rev.* **1999**, *99*, 3247–3276.
- (34) Rezac, J.; Hobza, P. Describing noncovalent interactions beyond the common approximations: How accurate is the gold standard, CCSD (T) at the complete basis set limit? *J. Chem. Theory Comput.* **2013**, *9*, 2151–2155.
- (35) Kubas, G. J. Metal-dihydrogen and σ -bond coordination: The consummate extension of the Dewar-Chatt-Duncanson model for metal-olefin π bonding. *J. Organomet. Chem.* **2001**, *635*, 37–68.
- (36) Kubas, G. J. Fundamentals of H₂ binding and reactivity on transition metals underlying hydrogenase function and H₂ production and storage. *Chem. Rev.* **2007**, *107*, 4152–4205.
- (37) Saillard, J. Y.; Hoffmann, R. Carbon-hydrogen and hydrogen-hydrogen activation in transition metal complexes and on surfaces. *J. Am. Chem. Soc.* **1984**, *106*, 2006–2026.
- (38) Runčevski, T.; Kapelewski, M. T.; Torres-Gavosto, R. M.; Tarver, J. D.; Brown, C. M.; Long, J. R. Adsorption of two gas molecules at a single metal site in a metalorganic framework. *Chem. Commun.* **2016**, *2*, 8251–8254.
- (39) Getman, R. B.; Miller, J. H.; Wang, K.; Snurr, R. Q. Metal alkoxide functionalization in metal-organic frameworks for enhanced ambient-temperature hydrogen storage. *J. Phys. Chem. C.* **2011**, *115*, 2066–2075.

- (40) Mardirossian, N.; Head-Gordon, M. ω B97M-V: A combinatorially optimized, range-separated hybrid, meta-GGA density functional with VV10 nonlocal correlation. *J. Chem. Phys.* **2016**, *144*.
- (41) Rappoport, D.; Furche, F. Property-optimized Gaussian basis sets for molecular response calculations. *J. Chem. Phys.* **2010**, *133*, 134105.
- (42) Getman, R. B.; Miller, J. H.; Wang, K.; Snurr, R. Q. Metal Alkoxide Functionalization in Metal-Organic Frameworks for Enhanced Ambient-Temperature Hydrogen Storage. *J. Phys. Chem. C* **2011**, *115*, 2066–2075.
- (43) Kemper, P. R.; Weis, P.; Bowers, M. T.; Maître, P. Origin of bonding interactions in $\text{Cu}^+(\text{H}_2)_n$ clusters: An experimental and theoretical investigation. *J. Am. Chem. Soc.* **1998**, *120*, 13494–13502.
- (44) Plitt, H. S.; Br, M. R.; Ahlrichs, R.; Schnckel, H. $[\text{Cu}(\text{2-H}_2)\text{Cl}]$, a Model Compound for H_2 Complexes. Ab Initio Calculations and Identification by IR Spectroscopy. *Angew. Chem., Int. Ed.* **1991**, *30*, 832–834.
- (45) Frohman, D. J.; Grubbs, G. S.; Yu, Z.; Novick, S. E. Probing the chemical nature of dihydrogen complexation to transition metals, a gas phase case study: $\text{H}_2\text{-CuF}$. *Inorg. Chem.* **2013**, *52*, 816–822.
- (46) Grubbs, G. S.; Obenchain, D. A.; Pickett, H. M.; Novick, S. E. $\text{H}_2\text{-AgCl}$: A spectroscopic study of a dihydrogen complex. *J. Chem. Phys.* **2014**, *141*.
- (47) Raghavachari, K.; Trucks, G. W.; Pople, J. A.; Head-Gordon, M. A fifth order comparison of electron correlation theories. *Chem. Phys. Lett.* **1989**, *157*, 479–483.
- (48) Pople, J. A.; Head-Gordon, M.; Fox, D. J.; Raghavachari, K.; Curtiss, L. A. Gaussian-1 theory: A general procedure for prediction of molecular energies. *J. Chem. Phys.* **1989**, *90*, 5622–5629.

- (49) Curtiss, L. A.; Raghavachari, K.; Trucks, G. W.; Pople, J. A. Gaussian-2 theory for molecular energies of first- and second-row compounds. *J. Chem. Phys.* **1991**, *94*, 7221–7230.
- (50) Curtiss, L. A.; Raghavachari, K.; Redfern, P. C.; Rassolov, V.; Pople, J. A. Gaussian-3 (G3) theory for molecules containing first and second-row atoms. *J. Chem. Phys.* **1998**, *109*, 7764–7776.
- (51) Curtiss, L. A.; Redfern, P. C.; Raghavachari, K. Gaussian-4 theory. *J. Chem. Phys.* **2007**, *126*.
- (52) Martin, J. M.; De Oliveira, G. Towards standard methods for benchmark quality ab initio thermochemistry - W1 and W2 theory. *J. Chem. Phys.* **1999**, *111*, 1843–1856.
- (53) Daniel Boese, A.; Oren, M.; Atasoylu, O.; Martin, J. M.; Kállay, M.; Gauss, J. W3 theory: Robust computational thermochemistry in the kJ/mol accuracy range. *J. Chem. Phys.* **2004**, *120*, 4129–4141.
- (54) Karton, A.; Rabinovich, E.; Martin, J. M.; Ruscic, B. W4 theory for computational thermochemistry: In pursuit of confident sub-kJ/mol predictions. *J. Chem. Phys.* **2006**, *125*, 11599.
- (55) Tajti, A.; Szalay, P. G.; Császár, A. G.; Kállay, M.; Gauss, J.; Valeev, E. F.; Flowers, B. A.; Vázquez, J.; Stanton, J. F. HEAT: High accuracy extrapolated ab initio thermochemistry. *J. Chem. Phys.* **2004**, *121*, 11599–11613.
- (56) DeYonker, N. J.; Cundari, T. R.; Wilson, A. K. The correlation consistent composite approach (ccCA): An alternative to the Gaussian-n methods. *J. Chem. Phys.* **2006**, *124*, 84108.
- (57) East, A. L. L.; Allen, W. D. The heat of formation of NCO. *J. Chem. Phys.* **1993**, *99*, 4638–4650.

- (58) Császár, A. G.; Allen, W. D.; Schaefer, H. F. In pursuit of the ab initio limit for conformational energy prototypes. *J. Chem. Phys.* **1998**, *108*, 9751–9764.
- (59) Helgaker, T.; Klopper, W.; Koch, H.; Noga, J. Basis-set convergence of correlated calculations on water. *J. Chem. Phys.* **1997**, *106*, 9639–9646.
- (60) Dunning, T. H. Gaussian basis sets for use in correlated molecular calculations. I. The atoms boron through neon and hydrogen. *J. Chem. Phys.* **1989**, *90*, 1007–1023.
- (61) Woon, D. E.; Dunning, T. H. Gaussian basis sets for use in correlated molecular calculations. III. The atoms aluminum through argon. *J. Chem. Phys.* **1993**, *98*, 1358–1371.
- (62) Woon, D. E.; Dunning, T. H. Gaussian basis sets for use in correlated molecular calculations. V. Core-valence basis sets for boron through neon. *J. Chem. Phys.* **1995**, *103*, 4572–4585.
- (63) Peterson, K. A.; Dunning, T. H. Accurate correlation consistent basis sets for molecular core-valence correlation effects: The second row atoms Al–Ar, and the first row atoms B–Ne revisited. *J. Chem. Phys.* **2002**, *117*, 10548–10560.
- (64) Balabanov, N. B.; Peterson, K. A. Systematically convergent basis sets for transition metals. I. All-electron correlation consistent basis sets for the 3d elements Sc–Zn. *J. Chem. Phys.* **2005**, *123*, 64107.
- (65) Jensen, F. Atomic orbital basis sets. *Wiley Interdiscip. Rev.: Comput. Mol. Sci.* **2013**, *3*, 273–295.
- (66) Pulay, P.; Hamilton, T. P. UHF natural orbitals for defining and starting MC-SCF calculations. *J. Chem. Phys.* **1988**, *88*, 4926–4933.

- (67) Bofill, J. M.; Pulay, P. The unrestricted natural orbital-complete active space (UNO-CAS) method: An inexpensive alternative to the complete active space-self-consistent-field (CAS-SCF) method. *J. Chem. Phys.* **1989**, *90*, 3637–3646.
- (68) Gill, P. M.; Johnson, B. G.; Pople, J. A. A standard grid for density functional calculations. *Chem. Phys. Lett.* **1993**, *209*, 506–512.
- (69) Bhatia, S. K.; Myers, A. L. Optimum conditions for adsorptive storage. *Langmuir* **2006**, *22*, 1688–1700.
- (70) Bae, Y. S.; Snurr, R. Q. Optimal isosteric heat of adsorption for hydrogen storage and delivery using metal-organic frameworks. *Microporous Mesoporous Mater.* **2010**, *132*, 300–303.
- (71) Cybulski, S. M.; Lytle, M. L. The origin of deficiency of the supermolecule second-order Møller-Plesset approach for evaluating interaction energies. *J. Chem. Phys.* **2007**, *127*, 141102.
- (72) Jurečka, P.; Šponer, J.; Černý, J.; Hobza, P. Benchmark database of accurate (MP2 and CCSD(T) complete basis set limit) interaction energies of small model complexes, DNA base pairs, and amino acid pairs. *Phys. Chem. Chem. Phys.* **2006**, *8*, 1985–1993.
- (73) Perdew, J. P.; Ruzsinszky, A.; Tao, J.; Staroverov, V. N.; Scuseria, G. E.; Csonka, G. I. Prescription for the design and selection of density functional approximations: More constraint satisfaction with fewer fits. *J. Chem. Phys.* **2005**, *123*, 62201.
- (74) Vosko, S. H.; Wilk, L.; Nusair, M. Accurate spin-dependent electron liquid correlation energies for local spin density calculations: a critical analysis. *Can. J. Phys.* **1980**, *58*, 1200–1211.
- (75) Perdew, J. P.; Wang, Y. Accurate and simple analytic representation of the electron-gas correlation energy. *Phys. Rev. B* **1992**, *45*, 13244.

- (76) Perdew, J. P.; Burke, K.; Ernzerhof, M. Generalized gradient approximation made simple. *Phys. Rev. Lett.* **1996**, *77*, 3865.
- (77) Grimme, S.; Antony, J.; Ehrlich, S.; Krieg, H. A consistent and accurate ab initio parametrization of density functional dispersion correction (DFT-D) for the 94 elements H-Pu. *J. Chem. Phys.* **2010**, *132*, 154104.
- (78) Hammer, B.; Hansen, L. B.; Nørskov, J. K. Improved adsorption energetics within density-functional theory using revised Perdew-Burke-Ernzerhof functionals. *Phys. Rev. B* **1999**, *59*, 7413.
- (79) Zhang, Y.; Yang, W. Comment on Generalized gradient approximation made simple. *Phys. Rev. Lett.* **1998**, *80*, 890.
- (80) Witte, J.; Mardirossian, N.; Neaton, J. B.; Head-Gordon, M. Assessing DFT-D3 Damping Functions Across Widely Used Density Functionals: Can We Do Better? *J. Chem. Theory Comput.* **2017**, *13*, 2043–2052.
- (81) Becke, A. D. Density-functional exchange-energy approximation with correct asymptotic behavior. *Phys. Rev. A* **1988**, *38*, 3098.
- (82) Lee, C.; Yang, W.; Parr, R. G. Development of the Colle-Salvetti correlation-energy formula into a functional of the electron density. *Phys. Rev. B* **1988**, *37*, 785–789.
- (83) Becke, A. D. Density-functional thermochemistry. V. Systematic optimization of exchange-correlation functionals. *J. Chem. Phys.* **1997**, *107*, 8554–8560.
- (84) Grimme, S.; Ehrlich, S.; Goerigk, L. Effect of the damping function in dispersion corrected density functional theory. *J. Comput. Chem.* **2011**, *32*, 1456–1465.
- (85) Haoyu, S. Y.; Zhang, W.; Verma, P.; He, X.; Truhlar, D. G. Nonseparable exchange–correlation functional for molecules, including homogeneous catalysis involving transition metals. *Phys. Chem. Chem. Phys.* **2015**, *17*, 12146–12160.

- (86) Perdew, J. P.; Chevary, J. A.; Vosko, S. H.; Jackson, K. A.; Pederson, M. R.; Singh, D. J.; Fiolhais, C. Atoms, molecules, solids, and surfaces: Applications of the generalized gradient approximation for exchange and correlation. *Phys. Rev. B* **1992**, *46*, 6671–6687.
- (87) Perdew, J. P. Density-functional approximation for the correlation energy of the inhomogeneous electron gas. *Phys. Rev. B* **1986**, *33*, 8822.
- (88) Tao, J.; Perdew, J. P.; Staroverov, V. N.; Scuseria, G. E. Climbing the density functional ladder: Nonempirical meta-generalized gradient approximation designed for molecules and solids. *Phys. Rev. Lett.* **2003**, *91*, 146401.
- (89) Perdew, J. P.; Ruzsinszky, A.; Csonka, G. I.; Constantin, L. A.; Sun, J. Workhorse semilocal density functional for condensed matter physics and quantum chemistry. *Phys. Rev. Lett.* **2009**, *103*, 026403.
- (90) Sun, J.; Ruzsinszky, A.; Perdew, J. P. Strongly constrained and appropriately normed semilocal density functional. *Phys. Rev. Lett.* **2015**, *115*, 036402.
- (91) Brandenburg, J.; Bates, J.; Sun, J.; Perdew, J. Benchmark tests of a strongly constrained semilocal functional with a long-range dispersion correction. *Phys. Rev. B* **2016**, *94*, 115144.
- (92) Mardirossian, N.; Head-Gordon, M. Mapping the genome of meta-generalized gradient approximation density functionals: The search for B97M-V. *J. Chem. Phys.* **2015**, *142*, 074111.
- (93) Mardirossian, N.; Ruiz Pestana, L.; Womack, J. C.; Skylaris, C.-K.; Head-Gordon, T.; Head-Gordon, M. Use of the rVV10 nonlocal correlation functional in the B97M-V density functional: defining B97M-rV and related functionals. *J. Phys. Chem. Lett.* **2016**, *8*, 35–40.

- (94) Sabatini, R.; Gorni, T.; De Gironcoli, S. Nonlocal van der Waals density functional made simple and efficient. *Phys. Rev. B* **2013**, *87*, 4–7.
- (95) Wellendorff, J.; Lundgaard, K. T.; Jacobsen, K. W.; Bligaard, T. mBEEF: An accurate semi-local Bayesian error estimation density functional. *J. Chem. Phys.* **2014**, *140*, 144107.
- (96) Zhao, Y.; Truhlar, D. G. A new local density functional for main-group thermochemistry, transition metal bonding, thermochemical kinetics, and noncovalent interactions. *J. Chem. Phys.* **2006**, *125*, 194101.
- (97) Yu, H. S.; He, X.; Truhlar, D. G. MN15-L: A new local exchange-correlation functional for Kohn–Sham density functional theory with broad accuracy for atoms, molecules, and solids. *J. Chem. Theory Comput.* **2016**, *12*, 1280–1293.
- (98) Sun, J.; Haunschild, R.; Xiao, B.; Bulik, I. W.; Scuseria, G. E.; Perdew, J. P. Semilocal and hybrid meta-generalized gradient approximations based on the understanding of the kinetic-energy-density dependence. *J. Chem. Phys.* **2013**, *138*, 044113.
- (99) Becke, A. D. A new mixing of Hartree–Fock and local density-functional theories. *J. Chem. Phys.* **1993**, *98*, 1372–1377.
- (100) Adamo, C.; Barone, V. Toward reliable density functional methods without adjustable parameters: The PBE0 model. *J. Chem. Phys.* **1999**, *110*, 6158–6170.
- (101) Staroverov, V. N.; Scuseria, G. E.; Tao, J.; Perdew, J. P. Comparative assessment of a new nonempirical density functional: Molecules and hydrogen-bonded complexes. *J. Chem. Phys.* **2003**, *119*, 12129–12137.
- (102) Hui, K.; Chai, J.-D. SCAN-based hybrid and double-hybrid density functionals from models without fitted parameters. *J. Chem. Phys.* **2016**, *144*, 044114.

- (103) Becke, A. D. Densityfunctional thermochemistry. III. The role of exact exchange. *J. Chem. Phys.* **1993**, *98*, 5648–5652.
- (104) Zhao, Y.; Truhlar, D. G. The M06 suite of density functionals for main group thermochemistry, thermochemical kinetics, noncovalent interactions, excited states, and transition elements: two new functionals and systematic testing of four M06-class functionals and 12 other functionals. *Theor. Chem. Acc.* **2008**, *120*, 215–241.
- (105) Wang, Y.; Verma, P.; Jin, X.; Truhlar, D. G.; He, X. Revised M06 density functional for main-group and transition-metal chemistry. *Proc. Natl. Acad. Sci. U. S. A.* **2018**, *115*, 10257–10262.
- (106) Haoyu, S. Y.; He, X.; Li, S. L.; Truhlar, D. G. MN15: A Kohn–Sham global-hybrid exchange–correlation density functional with broad accuracy for multi-reference and single-reference systems and noncovalent interactions. *Chem. Sci.* **2016**, *7*, 5032–5051.
- (107) Sun, J.; Perdew, J. P.; Ruzsinszky, A. Semilocal density functional obeying a strongly tightened bound for exchange. *Proc. Natl. Acad. Sci. U. S. A.* **2015**, *112*, 685–689.
- (108) Gill, P. M.; Adamson, R. D.; Pople, J. A. Coulomb-attenuated exchange energy density functionals. *Mol. Phys.* **1996**, *88*, 1005–1009.
- (109) Leininger, T.; Stoll, H.; Werner, H.-J.; Savin, A. Combining long-range configuration interaction with short-range density functionals. *Chem. Phys. Lett.* **1997**, *275*, 151–160.
- (110) Chai, J.-D.; Head-Gordon, M. Long-range corrected hybrid density functionals with damped atom–atom dispersion corrections. *Phys. Chem. Chem. Phys.* **2008**, *10*, 6615–6620.
- (111) Chai, J.-D.; Head-Gordon, M. Systematic optimization of long-range corrected hybrid density functionals. *J. Chem. Phys.* **2008**, *128*, 084106.

- (112) Lin, Y.-S.; Li, G.-D.; Mao, S.-P.; Chai, J.-D. Long-range corrected hybrid density functionals with improved dispersion corrections. *J. Chem. Theory Comput.* **2012**, *9*, 263–272.
- (113) Mardirossian, N.; Head-Gordon, M. ω B97X-V: A 10-parameter, range-separated hybrid, generalized gradient approximation density functional with nonlocal correlation, designed by a survival-of-the-fittest strategy. *Phys. Chem. Chem. Phys.* **2014**, *16*, 9904–9924.
- (114) Peverati, R.; Truhlar, D. G. Improving the accuracy of hybrid meta-GGA density functionals by range separation. *J. Phys. Chem. Lett.* **2011**, *2*, 2810–2817.
- (115) Verma, P.; Wang, Y.; Ghosh, S.; He, X.; Truhlar, D. G. Revised M11 Exchange-Correlation Functional for Electronic Excitation Energies and Ground-State Properties. *J. Phys. Chem. A* **2019**, *123*, 2966–2990.
- (116) Krukau, A. V.; Vydrov, O. A.; Izmaylov, A. F.; Scuseria, G. E. Influence of the exchange screening parameter on the performance of screened hybrid functionals. *J. Chem. Phys.* **2006**, *125*, 224106.
- (117) Henderson, T. M.; Janesko, B. G.; Scuseria, G. E. Generalized gradient approximation model exchange holes for range-separated hybrids. *J. Chem. Phys.* **2008**, *128*, 194105.
- (118) Peverati, R.; Truhlar, D. G. Screened-exchange density functionals with broad accuracy for chemistry and solid-state physics. *Phys. Chem. Chem. Phys.* **2012**, *14*, 16187–16191.
- (119) Seidl, A.; Görling, A.; Vogl, P.; Majewski, J. A.; Levy, M. Generalized Kohn-Sham schemes and the band-gap problem. *Phys. Rev. B* **1996**, *53*, 3764–3774.
- (120) Grimme, S. Semiempirical hybrid density functional with perturbative second-order correlation. *J. Chem. Phys.* **2006**, *124*, 6158.

- (121) Brmond, E.; Adamo, C. Seeking for parameter-free double-hybrid functionals: The PBE0-DH model. *J. Chem. Phys.* **2011**, *135*, 024106.
- (122) Zhang, Y.; Xu, X.; Goddard, W. A. Doubly hybrid density functional for accurate descriptions of nonbond interactions, thermochemistry, and thermochemical kinetics. *Proc. Natl. Acad. Sci. U. S. A.* **2009**, *106*, 4963–4968.
- (123) Mardirossian, N.; Head-Gordon, M. Survival of the most transferable at the top of Jacob’s ladder: Defining and testing the ω B97M(2) double hybrid density functional. *J. Chem. Phys.* **2018**, *148*, 241736.
- (124) Zhang, I. Y.; Xu, X.; Jung, Y.; Goddard, W. A. A fast doubly hybrid density functional method close to chemical accuracy using a local opposite spin ansatz. *Proc. Natl. Acad. Sci. U. S. A.* **2011**, *108*, 19896–19900.
- (125) Kozuch, S.; Martin, J. M. L. Spin-component-scaled double hybrids: An extensive search for the best fifth-rung functionals blending DFT and perturbation theory. *J. Comput. Chem.* **2013**, *34*, 2327–2344.
- (126) Goerigk, L.; Grimme, S. Efficient and accurate double-hybrid-meta-GGA density functionals- evaluation with the extended GMTKN30 database for general main group thermochemistry, kinetics, and noncovalent interactions. *J. Chem. Theory Comput.* **2011**, *7*, 291–309.
- (127) Manzer, S.; Horn, P. R.; Mardirossian, N.; Head-Gordon, M. Fast, accurate evaluation of exact exchange: The occ-RI-K algorithm. *J. Chem. Phys.* **2015**, *143*, 24113.
- (128) Manzer, S. F.; Epifanovsky, E.; Head-Gordon, M. Efficient implementation of the pair atomic resolution of the identity approximation for exact exchange for hybrid and range-separated density functionals. *J. Chem. Theory Comput.* **2015**, *11*, 518–527.

- (129) Ochsenfeld, C.; White, C. A.; Head-Gordon, M. Linear and sublinear scaling formation of Hartree-Fock-type exchange matrices. *J. Chem. Phys.* **1998**, *109*, 1663–1669.
- (130) Chan, B.; Gill, P. M. W.; Kimura, M. Assessment of DFT Methods for Transition Metals with the TMC151 Compilation of Data Sets and Comparison with Accuracies for Main-Group Chemistry. *J. Chem. Theory Comput.* **2019**, *15*, 3622.
- (131) Grimme, S. Accurate description of van der Waals complexes by density functional theory including empirical corrections. *J. Comput. Chem.* **2004**, *25*, 1463–1473.
- (132) Grimme, S. Semiempirical GGA-type density functional constructed with a long-range dispersion correction. *J. Comput. Chem.* **2006**, *27*, 1787–1799.
- (133) Dion, M.; Rydberg, H.; Schröder, E.; Langreth, D. C.; Lundqvist, B. I. Van der Waals density functional for general geometries. *Phys. Rev. Lett.* **2004**, *92*.
- (134) Klimeš, J.; Bowler, D. R.; Michaelides, A. Chemical accuracy for the van der Waals density functional. *J. Phys.: Condens. Matter* **2009**, *22*, 022201.
- (135) Carrete, J.; Longo, R.; Gallego, L.; Vega, A.; Balbás, L. Al enhances the H₂ storage capacity of graphene at nanoribbon borders but not at central sites: a study using nonlocal van der Waals density functionals. *Phys. Rev. B* **2012**, *85*, 125435.
- (136) Xu, L.; Ge, Q. Effect of defects and dopants in graphene on hydrogen interaction in graphene-supported NaAlH₄. *Int. J. Hydrogen Energy* **2013**, *38*, 3670–3680.
- (137) Lebon, A.; Carrete, J.; Gallego, L.; Vega, A. Ti-decorated zigzag graphene nanoribbons for hydrogen storage. A van der Waals-corrected density-functional study. *Int. J. Hydrogen Energy* **2015**, *40*, 4960–4968.
- (138) Kocman, M.; Jurečka, P.; Dubecký, M.; Otyepka, M.; Cho, Y.; Kim, K. S. Choosing a density functional for modeling adsorptive hydrogen storage: reference quantum

- mechanical calculations and a comparison of dispersion-corrected density functionals. *Phys. Chem. Chem. Phys.* **2015**, *17*, 6423–6432.
- (139) Fornace, M. E.; Lee, J.; Miyamoto, K.; Manby, F. R.; Miller, T. F. Embedded mean-field theory. *J. Chem. Theory Comput.* **2015**, *11*, 568–580.
- (140) Ding, F.; Manby, F. R.; Miller, T. F. Embedded Mean-Field Theory with Block-Orthogonalized Partitioning. *J. Chem. Theory Comput.* **2017**, *13*, 1605–1615.
- (141) Veccham, S. P.; Lee, J.; Head-Gordon, M. Making many-body interactions nearly pairwise additive: The polarized many-body expansion approach. *J. Chem. Phys.* **2019**, *151*, 194101.
- (142) Boys, S. F.; Bernardi, F. d. The calculation of small molecular interactions by the differences of separate total energies. Some procedures with reduced errors. *Mol. Phys.* **1970**, *19*, 553–566.
- (143) Gráfová, L.; Pitonak, M.; Rezac, J.; Hobza, P. Comparative study of selected wave function and density functional methods for noncovalent interaction energy calculations using the extended S22 data set. *J. Chem. Theory and Comput.* **2010**, *6*, 2365–2376.
- (144) Řezáč, J.; Riley, K. E.; Hobza, P. S66: A well-balanced database of benchmark interaction energies relevant to biomolecular structures. *J. Chem. Theory Comput.* **2011**, *7*, 2427–2438.